The ORB2 RNA-binding protein negatively regulates its target transcripts during the Drosophila maternal-to-zygotic transition via its functionally conserved Zinc-binding 'ZZ' domain

Timothy C.H. Low[1], Hua Luo[1], Chalini Weerasooriya[2], Zhuyi Wang[1], Sichun Lin[3], Angelo Karaiskakis[1], Stephane Angers[2,3], Craig A. Smibert[1,2], Howard D. Lipshitz[1]*

[1]Department of Molecular Genetics, University of Toronto, 661 University Avenue, Toronto Ontario, Canada M5G 1M1

[2]Department of Biochemistry, University of Toronto, 661 University Avenue, Toronto Ontario, Canada M5G 1M1

[3]Department of Pharmaceutical Sciences & Donnelly Centre, University of Toronto, 160 College Street, Toronto, Ontario, Canada M5S 3E1

*Author for correspondence: howard.lipshitz@utoronto.ca

Running head: ORB2 negatively regulates mRNAs during the MZT

Keywords: ORB2, Cytoplasmic Polyadenylation Element Binding Protein (CPEB), RNA-binding protein (RBP), translational regulation, post-transcriptional regulation, pre-initiation complex (PIC), embryo, maternal-to-zygotic transition (MZT), S2 cell, Cup.

ARTICLE SUMMARY

We show that Drosophila ORB2, the ortholog of the human CPEB2 RNA-binding protein, negatively regulates its target mRNAs during the maternal-to-zygotic transition via its C-terminal Zinc-binding ('ZZ') domain.

ABSTRACT

Post-transcriptional regulation is particularly prominent during the maternal-to-zygotic transition (MZT), a developmental phase during which a large proportion of maternally provided mRNAs is repressed and cleared from metazoan embryos. RNA-binding proteins (RBPs) are key components of the post-transcriptional regulatory machinery. We show that the ORB2 RBP, the Drosophila ortholog of human Cytoplasmic Polyadenylation Element Binding Protein (hCPEB) 2-4 protein subfamily, binds to hundreds of maternally provided, rare-codon-enriched mRNAs in early embryos; that ORB2 targets are translationally repressed and unstable during the MZT; identify a U-rich motif enriched in ORB2 targets' 3′UTRs; and show that this motif confers ORB2 binding and repression to a luciferase reporter mRNA in S2 tissue culture cells. When tethered to a luciferase reporter, ORB2 and hCPEB2 (but not ORB and hCPEB1) repress translation; the C-terminal Zinc-binding ('ZZ') domain of ORB2 is necessary and sufficient for repression. ORB2 interacts with a suite of post-transcriptional regulators in early embryos; a subset of these interactions is lost upon deletion of the ZZ domain, notably with the Cup repressive complex. ORB2-targets significantly overlap with those previously identified for the repressive RBP, Smaug (SMG). Analysis of the early embryo's translatome in the presence or absence of the endogenous ZZ domain shows that mRNAs bound by ORB2 but not by SMG move onto polysomes upon ZZ domain deletion whereas co-bound transcripts do not, consistent with co-regulation of the latter set of transcripts by both RBPs. Our results assign a function to the ZZ domain and position ORB2 in the post-transcriptional network that regulates maternal transcripts during the Drosophila MZT.

INTRODUCTION

All animal embryos undergo a maternal-to-zygotic transition (MZT) that encompasses two global processes: First, a large subset of maternal gene products loaded into the egg by the female parent is cleared; second, the zygotic genome becomes transcriptionally active (TADROS

58 AND LIPSHITZ 2009; VASTENHOUW *et al.* 2019; HARRISON *et al.* 2023). In Drosophila embryos,
59 the MZT is both very rapid – reaching completion about 3 hours after fertilization – and
60 extensive: Thousands of maternally loaded transcripts are cleared (DE RENZIS *et al.* 2007;
61 LÉCUYER *et al.* 2007; TADROS *et al.* 2007; THOMSEN *et al.* 2010); hundreds of these transcripts
62 are translationally repressed (KRONJA *et al.* 2014); and thousands of genes are transcribed from
63 the embryo's own genome in a process known as zygotic genome activation (ZGA) (HARRISON
64 *et al.* 2023). Several RBPs have been shown to function in maternal transcript repression and
65 degradation in *Drosophila*: Smaug (SMG) directs repression and clearance of a subset of
66 maternal transcripts prior to ZGA (TADROS *et al.* 2007; CHEN *et al.* 2014); Brain tumor (BRAT)
67 binds to and represses a distinct subset of maternal mRNAs both before and after ZGA (LAVER
68 *et al.* 2015); Pumilio (PUM) co-binds a subset of the BRAT targets but primarily directs
69 transcript clearance after rather than before ZGA (THOMSEN *et al.* 2010; LAVER *et al.* 2015;
70 HAUGEN *et al.* 2024). In contrast to these 'repressive' RBPs, Rasputin (RIN), the Drosophila
71 ortholog of vertebrate G3BP, upregulates the stability and translation of its targets during the
72 MZT (LAVER *et al.* 2020a).
73 Here we focus on the ORB2 RBP, which is of particular interest because it and its
74 vertebrate homologs have been reported to mediate both negative and positive post-
75 transcriptional regulatory functions in a variety of organisms and cell types. ORB and ORB2 are
76 the fly homologs of the vertebrate Cytoplasmic Polyadenylation Element Binding (CPEB) family
77 of RBPs, which canonically interact with U-rich motifs known as cytoplasmic polyadenylation
78 elements (CPEs) in the 3′UTR of target transcripts (HAKE AND RICHTER 1994). Vertebrates have
79 four CPEBs (CPEB1-4), which can be divided into two groups based on sequence similarity: the
80 CPEB1-like subfamily (containing vertebrate CPEB1 and its homologs, such as Drosophila
81 ORB) and the CPEB2-like subfamily (containing vertebrate CPEB2-4 and their homologs, such
82 as Drosophila ORB2) (WANG AND COOPER 2009; FERNÁNDEZ-MIRANDA AND MÉNDEZ 2012;
83 IVSHINA *et al.* 2014; DURAN-ARQUÉ *et al.* 2022).
84 CPEB proteins are known to function in the regulation of cytoplasmic mRNAs involved in
85 egg maturation, embryonic stem cell division, memory formation, synaptic plasticity, and
86 gametogenesis (HAKE AND RICHTER 1994; GROISMAN *et al.* 2001; KELEMAN *et al.* 2007;
87 STANDART AND MINSHALL 2008; KRÜTTNER *et al.* 2012; XU *et al.* 2012). Xenopus CPEB1, for
88 example, is a major specificity factor of an mRNA masking complex that represses translation in

89 oocytes and mediates translational activation of its target mRNAs upon egg activation (HAKE
90 AND RICHTER 1994; KIM AND RICHTER 2006).
91 ORB2 has been shown to have a role in neural development, long-term memory formation,
92 and spermatogenesis (KELEMAN *et al.* 2007; HAFER *et al.* 2011; MAJUMDAR *et al.* 2012; XU *et al.*
93 2012; KHAN *et al.* 2015; HERVÁS *et al.* 2016). The *orb2* gene encodes two protein isoforms,
94 ORB2A and ORB2B, which have 542 amino acids in common (from N-to-C): a poly-glutamine
95 (polyQ) tract, a predicted intrinsically disordered region (IDR2) that spans approximately 200
96 amino acids, the RNA-binding domain (RBD) comprised of tandem RNA recognition motif
97 (RRM) domains, and a ZZ-class Zinc-binding domain. ORB2A and ORB2B differ only in IDR1
98 at their N-termini (ORB2B is diagrammed in Figure 1a). ORB2A-ORB2B hetero-oligomers
99 serve as translational activators whereas, in the absence of ORB2A, ORB2B does not readily
100 oligomerize and has been shown to repress translation of reporter transcripts *in vitro* and in S2
101 tissue culture cells (MASTUSHITA-SAKAI *et al.* 2010; KHAN *et al.* 2015; STEPIEN *et al.* 2016;
102 HERVAS *et al.* 2020). The early Drosophila embryo is unusual in that only one of the two protein
103 isoforms, ORB2B, is expressed, affording us the opportunity to assess ORB2B's mechanism of
104 action and function *in vivo* in the absence of ORB2A.
105 To identify protein and RNA components of ORB2B-containing ribonucleoprotein
106 complexes (RNPs) during the MZT, we used a synthetic antibody to immunoprecipitate (IP)
107 endogenously expressed ORB2-containing RNPs followed by either next-generation sequencing
108 of co-immunoprecipitated transcripts (RIP-seq) or mass spectrometry of associated proteins (IP-
109 MS). We show that ORB2 binds hundreds of mRNAs that are translationally repressed and
110 degraded during the MZT. These transcripts are enriched for rare codons in their open reading
111 frames and for a U-rich motif in their 3′UTRs. We identify over 200 protein binding partners of
112 ORB2, including components of the 43S translation pre-initiation complex (PIC) and the Cup-
113 ME31B-TRAL-BEL repressive complex (hereafter referred to as the Cup repressive complex).
114 We leverage cell culture assays to verify that ORB2 binding to the U-rich motif results in
115 translational repression of a reporter RNA; to map ORB2's repressive function to the C-terminal
116 ZZ domain; and to show that the repressive function of the ZZ domain is conserved in its
117 subfamily ortholog, human CPEB2 (hCPEB2), but not in members of the other subfamily, ORB
118 or hCPEB1. We produce a CRISPR deletion of the ZZ domain of endogenous ORB2 and show
119 that deletion of the ZZ domain results in loss of interaction with the PIC and the Cup repressive

120 complex and a shift of ORB2's targets onto polysomes in early embryos. We show that a subset
121 of ORB2's targets is co-bound by the SMG RBP. Loss of the ZZ domain results in 'ORB2 only'
122 targets (i.e., those not co-bound by SMG) moving onto polysomes; in contrast, ORB2-SMG co-
123 bound targets do not. Together our results provide a function for the ZZ domain and position
124 ORB2 within the RBP regulatory network that controls the post-transcriptional fate of maternal
125 mRNAs. We report elsewhere that the endogenous deletion of the ZZ domain leads to defects in
126 spermatogenesis (LOW *et al.* 2025) and brain development (HAILSTOCK *et al.* 2025).
127

128 **MATERIALS AND METHODS**

129

130 **Drosophila stocks**

131 The following *Drosophila melanogaster* stocks were used: w^{1118} and $orb^{\Delta ZZ}$. The latter
132 stock was generated for use in this study (see below). Flies were cultivated at 25°C under
133 standard laboratory conditions unless otherwise indicated.
134

135 **Generation of the CRISPR deletion of the ZZ domain at the ORB2 endogenous locus**

136 Generation of this CRISPR line was performed by Well Genetics (13F.-12, No. 93, Sec. 1,
137 Xintai 5th Rd., Xizhi Dist., New Taipei City 221416, Taiwan (R.O.C.)). The scarless PBac-
138 dsRed method was used to produce the $orb2^{\Delta ZZ}$ line (GRATZ *et al.* 2013; GRATZ *et al.* 2014). The
139 ZZ domain, defined as from D638 to C704 (using the numbering from the ORB2-PB isoform)
140 was targeted for deletion such that the endogenous 3'UTR was retained in its entirety. Two guide
141 RNAs (gRNAs) were used to direct CRISPR to make double-stranded cuts in the DNA
142 surrounding the mutation of interest; in our case, one gRNA was directed to the genome to a cut
143 site just after the beginning of the ZZ domain (-179 nt from STOP Codon of *orb2-RA/B/C/D/H*),
144 and the second gRNA was directed to cut +3 nt from STOP Codon. Cas9 mediates breaks in the
145 double-stranded DNA, which triggers homologous repair between the genomic locus and a donor
146 plasmid, which was co-injected with the gRNA plasmid.

147 The donor plasmid containing the mutation of interest (a deletion of the ZZ domain, which
148 removes the genomic portion of the coding sequence after the end of the second RRM,
149 advancing the STOP codon to this point, such that this mutant protein would stop at residue
150 L637 in the PB isoform) followed by a dsRed marker flanked by Piggy Bac 5′ terminal repeats

151 (Figure S1a). The Piggy Bac transposon terminal repeats enabled this marker to be excised after
152 it had been used to screen for successful CRISPR incorporation into the genome, leaving behind
153 no trace of the marker afterwards (i.e. it is "scarless" on the genome). Flanking this dsRed
154 marker is genomic sequence that is homologous to the base genome, 1kb upstream and
155 downstream for the cut site; this provided the homology needed to facilitate homology-
156 dependent repair (HDR) between the donor plasmid and the genomic site.
157 After injection of the host w^{1118} strain (LWG182), balanced fly lines were established from
158 the resulting progeny and screened for successful integration of the mutation-containing region
159 of the donor plasmid. Successful recombination resulted in an ORB2 gene locus harboring a
160 precise deletion of the ZZ domain at the endogenous locus, marked by the expression of dsRed,
161 which was later removed from the genome using the Piggy Bac transposon machinery to excise
162 the marker by crossing them to a Piggy Bac expressing fly (BDSC #8285). PCR was carried out
163 to confirm donor plasmid insertion at the intended location in the correct orientation (Figure S1b)
164 followed by deletion of the dsRed marker (Figure S1c), which was then verified by sequencing
165 (Figure S2). PCR was used to confirm that the $orb2^{\Delta ZZ}$ line was not infected with Wolbachia
166 (since BDSC #8285 is known to be infected) (data not shown).
167
168 **Synthetic antibody (Fab) expression and harvesting**
169 Phage displayed synthetic antibodies against ORB2 protein have been described previously
170 (LAVER *et al.* 2012; NA *et al.* 2016). To summarize, antigens containing amino acids 163-446
171 (numbered according to ORB2-PA isoform) were expressed and purified from *E. coli* as GST
172 fusion proteins. Synthetic antibody library F (LAVER *et al.* 2012; NA *et al.* 2016) was used in five
173 rounds of binding selection, which included negative selection to remove antibodies that bound
174 to GST, to obtain synthetic antibodies that bound to the ORB2 antigen. The two synthetic
175 antibodies used in this study were anti-ORB2 E8 and anti-hEGFR C1 (control).
176 Synthetic antibodies ('Fabs') were expressed and harvested from *E. coli* as previously
177 described (LAVER *et al.* 2012). In summary, DH5α *E. coli* was transformed with plasmid
178 containing the FLAG- and 6xHis-tagged Fab open reading frame under the control of the *lac*
179 operator. Transformed cells were used to inoculate bacterial culture using 2xYT media; the
180 inoculated culture was incubated at 37°C on rotation at 225rpm until OD595 reached 0.8. The
181 culture was then induced with isopropyl β- d-1-thiogalactopyranoside (IPTG) to drive expression

182 of the Fab and allowed to grow at 18°C overnight on rotation at 225rpm. Bacteria were pelleted
183 by centrifugation at 4°C, 4000 rpm for 30 minutes, then the bacterial pellet was resuspended with
184 B-PER bacterial protein extraction reagent liquid solution (Thermo Scientific) supplemented
185 with protease inhibitors (150mM NaCl, 1mM AEBSF, 2mM Benzamidine, 2µg/mL Leupeptin,
186 2µg/mL Pepstatin) and Benzonase nuclease (2500 units/mL). Cells were allowed to lyse for 30
187 minutes at 4°C, then the lysate was cleared by centrifugation at 4°C at 21,380 RCF for 30
188 minutes. Supernatant was collected and synthetic antibodies were purified by passing lysates
189 through a column filled with Protein A affinity gel matrix beads; the captured Fab was eluted
190 with an acid buffer containing 50mM NaH_2PO_4, 100mM H_3PO_4, and 140mM NaCl, pH to 2.8 in
191 eight fractions of 200µL each. Fab-containing fractions were pooled and dialyzed with 1L PBS at
192 4°C for eight hours, twice. Dialyzed Fab was diluted with an equal volume of 95% glycerol
193 1xPBS and stored at -20°C.
194
195 **Collection of embryo lysates**
196 Lysate was collected from embryos laid and aged at 25°C. Extract was prepared from
197 embryos collected 0 to 3 hours post egg-lay on apple juice agar plates, dechorionated with 100%
198 bleach for 2 minutes, washed with 0.1% Triton X-100, and disrupted by crushing in minimal
199 volume of lysis buffer consisting of 150 mM KCl, 20 mM HEPES-KOH (pH 7.4), 1 mM $MgCl_2$,
200 1 mM DTT, and protease inhibitors (1 mM AEBSF, 2 mM benzamidine, 2 µg/mL pepstatin, 2
201 µg/mL leupeptin). The lysate was cleared by centrifugation at 4°C at 21,380 RCF for 15 minutes,
202 and the supernatant was collected and either used immediately or stored at -80°C.
203
204 **RIP-seq**
205 For each replicate of RIP-seq, 1mL of 0-3 hour embryo extract (prepared as described
206 above) was supplemented with Triton X-100 to 0.1% final concentration, then diluted in an equal
207 volume of lysis buffer with 0.1% Triton X-100 and cleared again by centrifugation at 4°C, 13
208 000 RPM for 15 minutes. The supernatant was incubated for 3 to 4 hours at 4°C with end-over-
209 end rotation with 100µL of anti-FLAG M2 affinity gel beads (Sigma) which had been pre-
210 incubated at 4°C with 50µg of purified anti-ORB2 E8 Fab blocked with 5µg/µL BSA. After
211 incubation, the lysates were decanted and beads were washed four times with lysis buffer
212 supplemented with 0.1% Triton X-100 and then three times with equilibration buffer: 100 mM

213 NaCl, 100 mM HEPES-NaOH (pH 7.4), 1 mM $MgCl_2$. Fabs and associated ribonucleoprotein
214 (RNPs) were eluted from the beads with 200 µL of 200µg/µL FLAG-peptide (Sigma) suspended
215 in equilibration buffer at 4°C for 20 minutes. RNA was isolated from the eluate using TRI
216 Reagent (Sigma) according to the manufacturer's instructions.
217 RNA was prepared for sequencing using Ribo-Zero Gold rRNA depletion kit and TruSeq
218 Stranded Total RNA Library Prep Kit (Illumina) according to manufacturer's instructions.
219 Libraries were sequenced using the HiSeq 2500 System, V4 Chemistry (Illumina), with paired-
220 end reads 125nt in length. The raw data are available on GEO (accession number GSE299661).
221
222 **Computational analysis of RIP-seq data**
223 Paired-end reads obtained from the sequencing were mapped to the *Drosophila*
224 *melanogaster* transcriptome r6.23, FB2018_04 obtained from flybase.org (OZTURK-COLAK *et al.*
225 2024) using the Salmon read mapping program (PATRO *et al.* 2017). The reference transcriptome
226 was supplied as a FASTA file. The resulting quantification was then analyzed for enrichment in
227 the ORB2 IP compared to Input and control IP compared to Input using the DESeq2 software
228 package for R (LOVE *et al.* 2014). Prior to formal analysis, the dataset was filtered for transcripts
229 having > 1TPM in at least three of the six samples, and rlog transformation was performed to
230 stabilize the variance. The similarity between samples was calculated by determining the Poisson
231 Distance between pairs of samples using the *PoiClaClu* package in R (see Figure S3) (WHITTEN
232 2011). The differential expression analysis was performed with the *dds* function using alpha =
233 0.01 cut-off for the False Discovery Rate. This returned a fold enrichment for each transcript,
234 accompanied by an adjusted *P*-value. We defined an ORB2-bound RNA target as satisfying all
235 three of the following criteria: (1) it was enriched in the ORB2 IP >1.5-fold relative to Input; (2)
236 it had an ORB2 IP/Control IP ratio >1.5; (3) it had an adjusted *P*-value < 0.05. The results are
237 presented in Figure 1 and File S1.
238 For comparisons between our dataset and previously published datasets, each pairwise
239 comparison was done independently. For comparisons that required a Wilcoxon Rank Sum test,
240 for each given pair of datasets, a common background list of genes was first compiled by taking
241 the intersection between the input/background of both datasets; genes which only appeared in
242 one dataset and not the other were discarded. Then, the measurements of the remaining identified
243 genes were placed into a dataframe in which each row corresponded to one unique gene, the first

244 column contained the measurements taken from one dataset, and the second column contained
245 measurements from the other dataset. This dataframe was then used to perform a Wilcoxon Rank
246 Sum test using the wilcox.test(x, y, exact = FALSE) function in R, where x is the data in the first
247 column, y is the data in the second column. The results are shown in Figure 2.
248 For comparisons that required a Fisher's Exact Test, for each given pair of datasets a
249 common background list of genes was first compiled by taking the intersection between the
250 input/background of both datasets; genes that only appeared in one dataset and not the other were
251 discarded. Then, the remaining identified genes of interest within in each dataset were compared
252 to look for common elements; genes that were identified in both lists of interest were annotated
253 as "Overlap", whereas genes that only appeared in one list were annotated as "X Only". A
254 Fisher's Exact Test was performed by using a 2x2 contingency table, where first cell (top left)
255 contained the number of genes that did not appear in either list (equal to the total number of
256 genes in the common background minus the number of genes described in the other three cells),
257 the second cell (top right) contained number of genes that appeared only on the ORB2 list
258 (ORB2 Only), the third cell (bottom left) contained the number of genes that appeared only on
259 the other list of interest (Other Only), and the last cell (bottom right) contained the number of
260 genes appear on both lists of interest (Overlap). This contingency table was constructed and
261 evaluated using the fisher.test() function in R. The results are presented in Table 1.
262 The Gene Ontology (GO) term enrichment analysis was performed using the Functional
263 Profiling function of the web version of gProfiler2 (accessed at https://biit.cs.ut.ee/gprofiler/gost)
264 (KOLBERG *et al.* 2023). The list of ORB2-bound target genes was provided to the program in the
265 Query field, and the Run Query option was selected in order to begin analysis. The results are
266 presented in Tables 2-4.
267
268 **Rare-codon enrichment analysis**
269 MELP score (SUPEK AND VLAHOVICEK 2005): Assuming ribosomal proteins are the best
270 translated and the most codon optimized genes in a given genome, a chi-square based statistic
271 called Measure Independent of Length and Composition (MILC) was calculated to evaluate the
272 difference of codon usage frequencies between ribosomal proteins and all annotated CDS that
273 are longer than 80 codons from Flybase 6.58. Then, MELP (MILC-based Expression Level
274 Predictor) was calculated based on MILC to predict expression level for each mRNA, and the

275 isoform with the minimum score (the worst predicted expression) was chosen to represent each
276 expressed gene (File S2). The Wilcoxon Rank Sum Test was performed for protein coding genes
277 that were either ORB2 target or non-target.
278 CAI (PUIGBO *et al.* 2008): Codon Adaptation Index (CAI) is another metric that evaluates
279 the similarity of codon usage to a reference set. This score was calculated for all annotated CDS
280 longer than 80 codons from Flybase 6.58 with the local version of CAIcal and the *Drosophila*
281 *melanogaster* codon usage table from the Kazusa codon usage database (NAKAMURA *et al.*
282 2000). The isoform with the minimum score (the most enriched for rare codons) was chosen to
283 represent each expressed gene (File S2), and the Wilcoxon Rank Sum Test was performed for
284 protein coding genes that were either ORB2 target or non-target.
285
286 **Number of Accessible Target Sites (#ATS) *de novo* motif discovery**
287 The ORB2 motifs were identified using the #ATS model, as described (LI *et al.* 2010).
288 Briefly, the #ATS program is a *de novo* motif discovery algorithm which takes as input nucleic
289 acid sequences belonging to mRNA transcripts in two lists: a positive (in this case, the 3′UTR of
290 ORB2 targets) and negative (in this case, the 3′UTR of co-expressed and unbound) list, and
291 outputs *k*-mers that best differentiate the positive transcripts from the negative transcripts. To
292 begin the analysis, 6-nt long seed sequences are first assessed based on their enrichment in the
293 positive list compared to the negative list, and then the top seed sequences are used as the
294 lauching point upon which the program iterates in an attempt to improve enrichment scores.This
295 is assessed based on enrichment in the positive list compared to the negative list and accounts for
296 RNA accessibility, as predicted by computational modeling of RNA secondary structures, and
297 assigned a *P*-value (see File S3). Iterative enrichment yielded degenerate motifs, so the top five
298 seed 6-mers from the #ATS were combined into a consensus sequence by aligning the G in the
299 motif and converting the resulting table into a position weight matrix (PWM) shown in Figure 3.
300
301 **Evaluation of ORB2 binding motif enrichment in RNA sequences**
302 The enrichment of ORB2 binding motifs was computationally evaluated using a multi-step
303 pipeline modified from our previous method, which assessed Smaug recognition element (SRE)
304 enrichment (CHEN *et al.* 2014). Briefly, the computation program scans each RNA using
305 RNAplfold (ViennaRNA package version 2.3.1) using parameters W=170 -L=120 -T=25

306 (BERNHART *et al.* 2006; LORENZ *et al.* 2011). Next, the nucleotide sequence is scanned for the
307 motif of interest (either the ORB2 motif uncovered by our analysis, NUUGUWU, or the ORB2
308 motif determined by RNA Compete, KUUUKKK) (RAY *et al.* 2013). At candidate motif sites,
309 the program then assesses the accessibility of the RNA at that position using the results from the
310 RNAplfold analysis. A score is then assigned to each motif site based on the probability that the
311 motif sequence is unpaired with any other nucleotide in the sequence. The total score for a
312 transcript is represented by the sum of motif scores for all motifs found in the sequence.
313
314 **Cell culture and transient transfection**
315 The Drosophila S2 cell line was maintained at 25°C with ExpressFive SFM (Fisher
316 Scientific) medium supplemented with 16mM L-glutamine, 100units/mL penicillin, and
317 100µg/mL streptomycin. 400µL of S2 cells at a density of 1.75×10^6 were plated into one well of
318 a 24-well tissue culture tray and transfected with a plasmid mixture containing 1.5ng firefly
319 luciferase plasmid, 1.5ng Renilla luciferase plasmid, 20ng FLAG-effector plasmid (containing
320 the open reading frame for either ORB2 whole protein, fragments of ORB2 protein, Protein A, or
321 GFP), 4ng of FLAG-GST plasmid, and 178.5ng pSP72 plasmid using 0.4µL of TransIT-Insect
322 transection reagent (Mirius Bio) suspended in 20µl of tissue culture medium according to the
323 manufacturer's instructions. For tethering assays, the luciferase plasmid was modified such that
324 the luciferase 3′UTR contained six copies of the TAR element and the effector protein construct
325 was modified to include the BIV-Tat ORF N-terminal to the FLAG tag. For experiments which
326 measure ORB2 binding to ORE elements, the luciferase plasmid was modified such that the
327 luciferase 3′UTR contained six copies of either intact ORE elements (UUUUGUU) or mutant
328 ORE elements (UUAUCUC). Both luciferase reporters were under the control of the metal-
329 inducible metallothionein promoter; all FLAG-tagged effector constructs were derived from
330 pAc5.1/V5-His plasmid (Thermo Fisher Scientific), which carries the Actin5C promoter.
331 Luciferase expression was induced 24 hours post-transfection by the addition of copper sulphate
332 to final concentration of 0.5mM. 24 hours post-induction and at 48 hours post-transfection cells
333 were harvested for downstream assays.
334
335 **Luciferase Assay**

336 Cell lysate was prepared from S2 cell transient transfections by dislodging cells from the
337 surfaces of the cell culture container and transferred into conical tubes. Cells were pelleted by
338 centrifugation at 21,380 RCF at 4°C for 1 minute; the supernatant was removed, and the cell
339 pellet was resuspended in by adding 20 µL of lysis buffer (containing 1xPassive Lysis Buffer
340 [Promega], 10 mg/mL BSA, and 1 mM AEBSF). Lysis was facilitated by pipetting up and down
341 and allowing the cells to lyse at 4°C for 10 minutes. Firefly and Renilla luciferase activities were
342 measured using the Dual-Luciferase Reporter Assay system (Promega) according to
343 manufacturer's instructions using a Berthold Detection Systems SIRIUS Luminometer.
344 Normalized luminescence values were calculated by first dividing the Firefly luminescence by
345 the Renilla luminesence readings to obtain a Firefly/Renilla ratio; ratios for each biological
346 replicate were obtained from the average of two technical replicates. Then, this ratio was
347 normalized to the corresponding GFP control sample (transfected in parallel to the experimental
348 conditions). Normalized expression was presented as the average of at least three biological
349 replicates with error bars representing standard deviation.
350
351 **Reverse Transcription – Quantitative Real-time Polymerase Chain Reaction (RT-qPCR)**
352 RNA isolated from ORB2 co-immunoprecipitations was reverse transcribed into single-
353 stranded cDNA with the Superscript IV reverse transcriptase kit (Invitrogen) according to
354 manufacturer's instructions. 500ng of total RNA per sample were used to synthesize cDNA,
355 which was primed using random hexamer primers. The resulting single-stranded cDNA was
356 diluted 1:25 using RNase-free water and used to perform quantitative real-time PCR (qPCR)
357 with primers specific to the various transcripts assayed. Primers were designed using NCBI
358 Primer-BLAST to cover all isoforms produced by a gene and were required to span an exon-
359 exon junction. qPCR was performed with SensiFAST SYBR PCR mix (Bioline) following the
360 manufacturer's protocol and using 5 µL of diluted cDNA per reaction. The CFX384 Real-Time
361 System (Bio-Rad) was used to carry out the PCR reaction.
362 The results of the qPCR were analyzed using CFX Manager software (Bio-Rad). Each
363 biological replicate represented a measurement obtained for a separate embryo collection; values
364 from three technical replicates were averaged and relative gene expression was normalized to the
365 ribosomal protein-coding transcript *RpL32*. Normalized expression was presented as the average
366 of three biological replicates with error bars representing standard deviation.

367

368 **Western Blots**

369 The following primary antibodies were used: mouse anti-ORB2 4GS (1:50) obtained from
370 the Developmental Studies Hybridoma Bank (https://dshb.biology.uiowa.edu/orb2-4G8) and
371 described in (HAFER *et al.* 2011), mouse M2 anti-FLAG (Sigma, 1:5,000), and mouse anti-Actin
372 (Sigma Cat#A4700, 1:10,000) which was used as a loading control.

373 Dechorionated embryos were counted, then lysed in Laemmli buffer at a concentration of 1
374 embryo/µL and boiled for 2 minutes. Proteins were resolved by loading 5µL of lysed embryos in
375 Laemmli buffer per lane into an SDS-PAGE and transferred to PVDF membrane in the absence
376 of SDS. The blot was blocked at room temperature with 2% non-fat milk in PBST for 30 minutes
377 and incubated with primary antibodies diluted in 2% non-fat milk in PBST at 4°C overnight.
378 After this incubation, the blot was washed 3 x 10 minutes with PBST at room temperature and
379 incubated with the appropriate HRP-conjugated secondary antibodies (1:5000, Jackson
380 ImmunoResearch) in 2% non-fat milk in PBST at room temperature for 1 hour. The blot was
381 washed 3 x 10 minutes with PBST and developed using Immobilon Luminata Crescendo
382 Western HRP substrate (Millipore), imaged using a BioRad Chemidoc MP Universal Hood III
383 imager and band intensities were quantified using ImageLab.

384

385 **Structure Prediction with AlphaFold**

386 For structural predictions the full amino acid sequence of the ZZ domain constructs used in
387 the tethering assays (see above) was predicted using AlphaFold version 3 (JUMPER *et al.* 2021;
388 ABRAMSON *et al.* 2024). Predictions were visualized and truncated to show regions A-to-D in
389 ChimeraX version 1.9 (MENG *et al.* 2023). Structures were color-coded to depict their predicted
390 local distance difference test (pLDDT) score using the AlphaFold Error Plot tool. The results are
391 presented in Figure S8.

392

393 **Mass spectrometry**

394 **Immunoprecipitation of ORB2 from embryo lysates with synthetic antibodies**

395 For IP-MS, 500 µL of 0-3 hour embryo extract (prepared as described above) was
396 supplemented with Triton X-100 to 0.1% final concentration, then diluted in an equal volume of
397 lysis buffer with 0.1% Triton X-100 and cleared again by centrifugation at 4°C at 21,380 RCF

398 for 15 minutes. The supernatant was incubated for 3 to 4 hours at 4°C with end-over-end rotation
399 with 100µL of anti-FLAG M2 affinity gel beads (Sigma) which had been pre-incubated at 4°C
400 with 50µg of purified anti-ORB2 E8 Fab blocked with 5µg/µL BSA. After incubation, the lysates
401 were decanted and beads were washed twice with lysis buffer supplemented with 0.1% Triton X-
402 100, then another twice with lysis buffer without Triton X-100; beads were transferred into a
403 new tube and washed another twice with lysis buffer without Triton X-100. Fabs and associated
404 proteins were eluted by tryptic digest: Beads were resuspended in 200 µL of 50mM ammonium
405 bicarbonate pH 8 supplemented with 2 µg of MS-grade trypsin and incubated at room
406 temperature overnight with end-over-end rotation. The digested peptides were collected and a
407 second elution with 200 µL of 50mM ammonium bicarbonate was performed at room
408 temperature for 30 minutes. The two fractions were pooled, flash frozen with dry ice, dehydrated
409 in a rotary evaporator for 8 hours, then stored at -20°C.
410
411 **Liquid chromatography and mass spectrometry**
412 For liquid chromatography (LC) the following solvents were used: Solvent A (0.1%
413 (vol/vol) formic acid) and Solvent B (0.1% (vol/vol) formic acid/90% (vol/vol) acetonitrile). The
414 LC parameters were set using an Easy-nLC 1200 instrument. Peptides were loaded and separated
415 on a nanoViper trap column (75µm x 2 cm), Acclaim PepMap 100 (C18, 3µm, 100 Å, Thermo
416 Scientific, cat. no. 164946), and EASY-Spray analytical column (75µm x 50cm) Acclaim
417 PepMap RSLC (C18, 2µm, 100Å, Thermo Scientific) using a flow rate of 225nL/minute.
418 Tandem MS was performed using the Q Exactive HF-Orbitrap mass spectrometer (Thermo
419 Scientific), as previously described (LIU *et al.* 2014; JIANG *et al.* 2015; CHIU *et al.* 2016). The
420 parameters for acquisition were 1 MS scan (50 ms; mass range, 390 to 1800) at a resolution of
421 60,000K, followed by up to 20 MS/MS scans (50 ms each) at a resolution of 15,000 and an AGC
422 target of 1x105. Candidate ions with charge states +2 to +7 were isolated using a window of 1.4
423 amu with a 5s dynamic exclusion window.
424
425 **Data processing and analysis**
426 Four biological replicates were performed, both in the presence or absence of RNase A.
427 The ProHits software package was used to perform Significance Analysis of INTeractome
428 (SAINT) in order to identify ORB2-interacting proteins (LIU *et al.* 2010; CHOI *et al.* 2012; LIU *et*

429 *al.* 2012). Proteins with associated peptide counts were filtered through the Trans Proteomic
430 Pipeline (TPP) for iProphet probability > 0.95 and number of unique peptides ≥ 2. SAINT
431 express analysis was performed on the ProHits interface with only Drosophila detected proteins
432 (selected options: number of compressed controls = 3, burn-in period, nburn = 2000; iterations,
433 niter = 5000, lowMode = 1; minFold = 1; normalize = 1; nCompressBaits = 3). This analysis
434 determined the probability of interaction for each identified prey protein. Proteins with AvgP
435 score ('SAINT score') ≥ 0.95 and BFDR ≤ 0.01 were defined as ORB2-ineracting proteins. Raw
436 data are available at MassIVE MSV000098275. The results are presented in File S4.
437 To perform network analysis on the list of identified protein interactors, we used the
438 GeneMANIA application (v3.5.2) (WARDE-FARLEY *et al.* 2010; FRANZ *et al.* 2018) with the
439 Cytoscape network visualization program (v3.9.1) (SHANNON *et al.* 2003; MONTOJO *et al.* 2010).
440 Data resulting from the IP-MS was imported to Cytoscape in table form. GeneMANIA maintains
441 a database of functional association data, which includes protein interactions, genetic
442 interactions, pathways, co-expression, and co-localization data that is obtained from a wide
443 variety of published sources. The details regarding the GeneMANIA database can be found
444 online (https://genemania.org/data/). Two interaction networks were produced by performing a
445 Network Search on a subset of identified protein interactors using GeneMANIA's *Drosophila*
446 *melanogaster* functional association database (see
447 https://genemania.org/data/current/Drosophila_melanogaster/ for details). Then, the nodes of
448 each network were annotated according to the association type reported in the GeneMANIA
449 database (i.e. known physical interaction, known genetic interaction, or predicted interaction).
450 The results are presented in Figure 5c,d.
451
452 **Embryo sample collection for *orb*$^{\Delta ZZ}$ time-course and polysome gradient RNA-seq**
453 **experiments**
454 Embryos were collected from *orb2*$^{\Delta ZZ}$ and *w*^{1118} (pre-injected control, LWG182) strains at
455 1-hour intervals post-egglay (0-1 hour, 1-2 hour, 2-3 hour), dechorionated with ice cold 100%
456 bleach for 2 minutes, washed with 0.1% Triton X-100, and disrupted by crushing using 0.5 g
457 embryos per mL of either lysis buffer (150 mM KCl, 20 mM HEPES-KOH (pH 7.4), 1 mM
458 MgCl2, 1 mM DTT, 1 mM AEBSF, 2 mM benzamidine, 2 µg/mL pepstatin, 2 µg/mL leupeptin)
459 or polysome lysis buffer (7.5 mM MgCl2, 500 mM NaCl, 25 mM Tris (pH 7.5), 1 mM DTT, 1

460 mM AEBSF, 2 µg/mL leupeptin, 2 mM benzamidine, 2 µg/mL pepstatin A, 2 mg/mL heparin,
461 0.5 mg/mL cycloheximide). The lysate with lysis buffer was cleared by centrifugation at 4°C at
462 21,380 RCF for 15 minutes, TRIzol (Invitrogen) was added to the supernatant which used
463 immediately for RNA extraction or stored at -80°C. The lysate with polysome lysis buffer was
464 either used immediately for polysome gradient processing or stored at -80°C.
465
466 **Polysome gradients**
467 The polysome gradient protocol was adapted from our published method with
468 modifications (CHEN *et al.* 2014). Lysed samples were diluted 1 in 10 in polysome lysis buffer
469 and 20% Triton X-100 was added to a final concentration of 1%, centrifuged at 6,000xg for 10
470 minutes and the resulting supernatant was diluted in polysome lysis buffer supplemented with
471 1% Triton X-100 to an A_{260} of 12.5. A 5 ml 15% to 45% linear sucrose gradient in 7.5 mM
472 $MgCl_2$, 500 mM NaCl, 50 mM Tris pH 7.5 was produced using a BioComp Model 117 Gradient
473 Mate gradient maker (Biocomp, Fredericton, New Brunswick, Canada) using a rotation angle of
474 86 degrees and a rotation speed of 25 for 51 seconds. After chilling the polysome gradient at 4ºC
475 for 1 hour, 200 µL of diluted embryo extract was loaded onto the top of the gradient, which was
476 then spun at 36,000 rpm in a Beckman SW50.1 rotor for 2.5 hours. 400 µL fractions (hand
477 fractionated) were collected, and A_{260} absorbance was measured using a Nanodrop (Thermo
478 Fisher Scientific). We added 20% SDS, 0.5 M EDTA and 20 mg/ml proteinase K to final
479 concentrations of 0.8%, 0.01 M and 0.128 mg/ml, respectively, and then incubated the fractions
480 for 30 minutes at 37ºC. 2.5 µL GlycoBlue (15 mg/mL, ThermoFisher) following which 2.5x
481 volume ethanol was added to each fraction and precipitated overnight. The resulting pellet was
482 washed with 75% ethanol and resuspended in phenol-saturated water.
483 The fractions were then separated into three pools: Pool 1 contained the (top) fractions 1-3,
484 pool 2 contained fractions 4-6, pool 3 contained fractions 7-13. Following two phenol-
485 chloroform extractions, the aqueous phase of each pool was collected with Invitrogen
486 Phasemaker Tubes (Fisher A33248) following the manufacturer's protocol. The samples were
487 precipitated by the addition of 7.5 M LiCl to a final concentration of 3.75 M followed by an
488 overnight incubation at -20°C. The pellets were washed with 70% ethanol and resuspended in
489 water.

490 RNA purification was performed using 2.2× volume NEBNext RNA Sample Purification
491 Beads (NEBNext Ultra II DNA Library Prep with Sample Purification Beads, E7767L)
492 following the manufacturer's protocol. RNA concentration was assessed with the Qubit RNA HS
493 Assay Kit (Thermo Fisher) and Agilent bioanalyzer at The Centre for Applied Genomics
494 (TCAG), The Hospital for Sick Children, Toronto, ON, Canada.
495
496 **rRNA depletion, library preparation and RNA-seq for time-course and polysome gradient**
497 **RNA-seq**
498 For the RNA-seq time-course rRNA depletion was performed as previously described
499 (HAUGEN *et al.* 2024). For polysome gradient RNA-seq, rRNA depletion was performed using
500 the QIAseq FastSelect rRNA Fly Kit (QIAGEN, Cat# 33326). Library preparation for RNA-seq
501 was conducted using the NEBNext Ultra II Directional RNA Library Prep Kit for Illumina, and
502 sequencing was performed on an Illumina NovaSeq 6000 (PE150) at the Next Generation
503 Sequencing Facility, The Centre for Applied Genomics (TCAG), The Hospital for Sick Children,
504 Toronto, ON, Canada.
505
506 **Computational analysis of time-course and polysome gradient RNA-seq data**
507 **RNA-seq data processing pipeline**
508 Adapter trimming and quality control used Trim Galore (Version 0.6.5)
509 [https://github.com/FelixKrueger/TrimGalore]. rRNA and 'unwanted' RNA removal used
510 SortMeRNA (version 2.1) (KOPYLOVA *et al.* 2012), filtering against *Drosophila melanogaster*
511 7SLRNA, rRNA, pseudogene-rRNA, tRNA, mtRNA and other species' rRNA databases.
512 Transcriptome alignment was carried out with Salmon (Version 1.9.1) (PATRO *et al.* 2017) in
513 mapping-based mode using FlyBase release 6.23 transcriptome RNA (FB2018_04) (OZTURK-
514 COLAK *et al.* 2024). Full decoy indexing was applied following the Salmon website instructions
515 [https://salmon.readthedocs.io/en/latest/salmon.html].
516
517 **Differential gene expression analysis**
518 Differential expression analysis used the R package tximeta (version 1.20.3) (LOVE *et al.*
519 2020) and Deseq2 (version 1.42.1) (LOVE *et al.* 2014) in R (version 4.3.2). For the *orb2*$^{\Delta ZZ}$ and
520 wild type time-course total RNA-seq, reads from each time point were normalized using the

521 DESeq2 package. For the *orb2*$^{\Delta ZZ}$ and wild type polysome gradient RNA-seq time-courses, reads
522 of each time point of *orb2*$^{\Delta ZZ}$ and wild type pool 1 and pool 3 RNA were normalized using the
523 DESeq2 package. For each gene, the mean of normalized counts per pool was computed at each
524 time point and genotype. The 'Translation Index' of each mRNA was calculated as the ratio =
525 mean normalized counts of pool 3 /mean normalized counts of pool 1. Normalized counts were
526 used for statistical analysis by the Wilcoxon Rank Sum Test and data were visualized with
527 ggplot2 in R. Raw data are available at GEO for the RNA-seq timecourse and polysome gradient
528 timecourse with accession numbers GSE299140 and GSE299019, respectively. The results are
529 presented in Figure 6 and Files S6 and S7.
530
531 **Comparisons between the ORB2 target list and published SMG, PUM, BRAT and RIN**
532 **target lists:**
533 The total list of genes detected in this ORB2 RIP-Seq experiment was first compared with
534 the total list of genes present in the published RIP-Chip experiments for SMG, PUM and BRAT
535 (CHEN *et al.* 2014; LAVER *et al.* 2015; LAVER *et al.* 2020a). The overlap between these lists was
536 retained, and the non-overlapping genes (i.e. genes detected in only one of the two experiments)
537 were discarded. From the remaining genes, ORB2 targets were compared with the targets of
538 SMG, PUM, and BRAT. The translation level, as defined by the polysome RIP-Seq ratio
539 measured in 0-1h embryos (see above), was compared for the overlap between the ORB target
540 list and the other list of interest (i.e. ORB2 + SMG co-targets, ORB2 + PUM co-targets, and
541 ORB2 + BRAT co-targets), and separately for the ORB2-only targets, the SMG- PUM-, and
542 BRAT-only targets, and non targets.
543
544 **RESULTS**
545
546 **ORB2 binds to over 450 targets in the early Drosophila embryo**
547 To identify transcripts that are bound by ORB2B (hereafter referred to as ORB2), we used
548 our previously produced Fab against an antigen N-terminal to the RRMs (Figure 1a) (LAVER *et*
549 *al.* 2012; NA *et al.* 2016) to perform RNA-coimmunoprecipitation (RIP) of endogenously
550 expressed ORB2 from embryo extracts prepared from 0-3 hour old embryos produced by w^{1118}
551 females. We enriched for mRNA in the sample by rRNA depletion, generated randomly primed

552 cDNA libraries from the resulting samples, and identified co-purifying RNAs by next-generation
553 RNA sequencing (see Materials and Methods). As a negative control, we performed parallel
554 RIPs using a control synthetic antibody, C1, as described previously (LAVER *et al.* 2015; LAVER
555 *et al.* 2020b; HAUGEN *et al.* 2024). Input samples from the same extracts were also sequenced.
556 We performed three biological replicates for each of these three conditions, for a total of nine
557 cDNA libraries.
558 To identify ORB2-bound target genes, we mapped the sequence reads to the Drosophila
559 transcriptome using Salmon read alignment software, and analyzed the results with the DESeq2
560 software package as described in Materials and Methods (LOVE *et al.* 2014; PATRO *et al.* 2017).
561 We defined an ORB2 target as a gene whose transcripts had fold enrichment >1.5 in the anti-
562 ORB2 RIP-seq compared to input and a ratio of ORB2/Control > 1.5, with an FDR adjusted *P*-
563 value < 0.05; using these criteria, we identified 462 genes whose transcripts were bound by
564 ORB2 (Figure 1b and File S1). ORB2's target transcripts were significantly less abundant than
565 co-expressed non-target transcripts (Figure 1c). RIP-RT-qPCR verified several of the target and
566 non-target RNAs (Figure 1d).
567 While ours is the first identification of ORB2 targets in embryos, there are previously
568 published target lists from other tissues or cells. For example, ORB2-bound transcripts were
569 identified in a CLIP experiment derived from ORB2 overexpression in S2 cells (STEPIEN *et al.*
570 2016). Of the 462 ORB2 targets on our list, 298 were identified in their CLIP-seq background set
571 of which they identified 113 as targets (Fisher's exact $P = 6.52 \times 10^{-7}$, Odds Ratio = 1.88). We
572 also examined the overlap of our targets with a list of ORB2-associated transcripts obtained by
573 performing RIP-seq on Drosophila head extracts (KOZLOV *et al.* 2023). 336 genes in our target
574 gene list overlapped with theirs (Fisher's exact $P < 10^{-15}$, Odds Ratio = 5.00).
575 The strong overlap between our ORB2 targets and previously reported targets from other
576 cell types/tissues verifies that our list is enriched for true ORB2 interactors.
577
578 **ORB2 targets are translationally repressed, deadenylated and degraded during the MZT**
579 To assess the post-transcriptional fate of ORB2 target transcripts in the early Drosophila
580 embryo, we utilized three previously published datasets that scored each transcript's translational
581 status, poly(A) tail length, and abundance during the MZT.

582 Two studies measured Translation Efficiency (TE), calculated from ribosome profiling,
583 during the MZT (DUNN *et al.* 2013; EICHHORN *et al.* 2016). At all three timepoints during the
584 MZT that were studied, ORB2 targets had a significantly lower TE compared to co-expressed,
585 non-target transcripts (Figure 2a-c). A third study measured Translation Index (TI), calculated as
586 the ratio of that transcript's abundance in polysome fractions of a sucrose gradient compared to
587 its abundance in non-polysomal fractions (CHEN *et al.* 2014). ORB2 targets had a significantly
588 lower TI than co-expressed non-target transcripts (Figure 2d).
589 We next assessed changes in poly(A) tail length and abundance for ORB2 targets between
590 the 0-1 hour timepoint and the 2-3 hour timepoint, which had been measured in parallel to TE
591 (EICHHORN *et al.* 2016). Decrease in abundance and poly(A) tail length were significantly greater
592 for ORB2 targets than for co-expressed, non-target transcripts (Figure 2e,f). We also examined
593 previously published lists of transcripts that are degraded during the MZT (Table 1). ORB2
594 targets overlapped significantly with transcripts identified to be unstable in activated eggs
595 (TADROS *et al.* 2007) (Fisher's Exact $P = 2.2 \times 10^{-16}$, odds ratio 3.85). In addition, ORB2 targets
596 were significantly enriched for genes that are degraded during the MZT (THOMSEN *et al.* 2010):
597 (Class III and V; respectively, Fisher's Exact $P = 0.02$, odds ratio 1.54 and Fisher's Exact $P =$
598 2.2×10^{-16}, odds ratio 2.54) and significantly depleted for transcripts that are stable (Class I;
599 Fisher's Exact $P = 2.2 \times 10^{-16}$, odds ratio 0.23).
600 We conclude that ORB2's target mRNAs are enriched for transcripts that are
601 translationally repressed, deadenylated and degraded during the MZT.
602
603 **ORB2 targets are enriched for rare codons**
604 It has previously been reported that ORB2 binds to and upregulates the stability and
605 translation of rare-codon-enriched mRNAs in neurons in *Drosophila* (STEWART *et al.* 2024). We,
606 therefore, asked whether ORB2's embryonic targets are enriched for rare codons. Two different
607 algorithms – MELP (SUPEK AND VLAHOVICEK 2005) and CAI (PUIGBO *et al.* 2008) – found
608 significant enrichment of rare codons in ORB2 targets relative to non-target, co expressed
609 mRNAs (Figure 2g,h and File S2). Why the post-transcriptional outcome in embryos is the
610 opposite of that in neurons will be considered in the Discussion.
611

612 **ORB2 targets are enriched for roles in gamete generation, gene regulation, and**
613 **development**
614 We next asked whether ORB2's targets were enriched for particular molecular, cellular or
615 biological functions by performing Gene Ontology (GO) term analysis using the gProfiler2 tool
616 (GENE ONTOLOGY *et al.* 2023; KOLBERG *et al.* 2023) (Tables 2-4).
617 The top GO terms under the Molecular Function category (Table 2) were dominated by
618 molecular binding functions; 'mRNA 3′UTR binding', and 'mRNA regulatory element binding'
619 were among the top ten results. Genes belonging to these terms included *orb2* itself as well as
620 *patronin, piwi,* and *bru1*. Other top terms included 'translation regulator activity' and 'translation
621 repressor activity'; genes belonging to these terms included *orb2* itself, *orb, pum, fmr1, sxl, heph,*
622 and *eIF4E-HP*. In the Biological Process category (Table 3), ORB2 targets were enriched for
623 terms related to regulation and development, such as 'anatomical structure development', 'cell
624 differentiation', and 'regulation of metabolic process'. ORB2 targets were also enriched for
625 terms related to gametogenesis, including 'gamete generation', 'oogenesis', and 'germ cell
626 development'. Genes related to these terms included *pum, rbfox1, piwi, heph, bru1, sxl,* and *mei-*
627 *P26*. Enrichment for GO terms related to gametogenesis in ORB2 targets is consistent with
628 previously reported functions for ORB2 in, for example, regulation of spermatogenesis (XU *et al.*
629 2012; GILMUTDINOV *et al.* 2021). The Cellular Component category (Table 4) was dominated by
630 terms that included 'ribonucleoprotein granule', 'P granule', 'pole plasm', and 'germ plasm'.
631 Genes related to these terms included *larp, tud, osk, tapas, ago1,* and *dcr-2*.
632 Many of the genes listed under enriched GO terms are previously identified ORB2 targets
633 (e.g., *orb2* itself, *ago1*, *bru1, dcr-2*, *eIF4E-HP*, *fmr1*, *heph*, *orb, pum, rbfox1, unr*)
634 (MASTUSHITA-SAKAI *et al.* 2010; XU *et al.* 2012; STEPIEN *et al.* 2016; KOZLOV *et al.* 2021) while
635 others are previously unidentified players in the same enriched function or process (e.g., *imp* and
636 *piwi*). Enrichment for mRNAs encoding known post-transcriptional regulators suggests that
637 ORB2 may play a key role in the cross-regulatory network that controls the MZT, a function that
638 is supported by our subsequent analyses reported below. The fact that ORB2 binds to and
639 potentially regulates mRNAs that encode other post-transcriptional regulators is also consistent
640 with a previous study in S2 cells showing that RNP complexes tend to be enriched for mRNAs
641 encoding post-transcriptional regulators (STOIBER *et al.* 2015).
642

643 **ORB2 target transcripts are enriched for a U-rich motif**

644 CPEB-family proteins are known to bind to U-rich elements, typically located in the
645 3′UTR of their mRNA targets (HAKE AND RICHTER 1994; DE MOOR AND RICHTER 1999; STEPIEN
646 *et al.* 2016). To predict *cis*-elements recognized by ORB2 from our *in vivo* RIP-seq results, we
647 used our algorithm, Number of Accessible Target Sites (#ATS), which performs *de novo* motif
648 discovery given a target set and a co-expressed non-target set of transcripts (LI *et al.* 2010) as
649 described in the Material and Methods. Using our input RNA-seq data, we identified the most
650 abundant transcript isoform from each expressed gene in the early embryo and then ran #ATS
651 analysis on the full-length transcripts or the 3′UTR sequences of ORB2 targets against non-
652 targets. Whereas no motif was produced from the analysis of full-length transcripts, the #ATS
653 program identified a list of 6-mers enriched in the 3′UTR of ORB2 target sequences relative to
654 non-targets; these 6-mers were then combined into a consensus motif (Figure 3a, File S3), which
655 will henceforth be referred to as an ORB2-recognition element (ORE: NUUGUWU (where W =
656 A or U). We also calculated an ORE 'score' for each transcript by summing the accessibilities of
657 each predicted ORE in that transcript (see Materials and Methods). ORB2 targets had
658 significantly higher ORE scores than co-expressed non-targets (Figure 3b, File S3).

659 This ORE is similar to published binding motifs: UUUU$(A)_{1\text{-}3}$U and UUUUGU identified
660 in S2 cells (STEPIEN *et al.* 2016); UUUURU (where R = A or G) in brain extracts (MASTUSHITA-
661 SAKAI *et al.* 2010); and KUUUKKK (where K = G or U) identified by an *in vitro* binding assay
662 (RAY *et al.* 2013). We calculated 'KUUUKKK' scores for each transcript and found that the
663 ORB2 targets we identified in the embryo have significantly higher scores than co-expressed
664 non-targets (Figure S3b, File S3).

665 The *de novo* discovery of the U-rich ORE enriched in ORB2 target RNAs in the early
666 embryo and its similarity to ORB2 motifs previously identified using a variety of methods
667 supports the conclusion that our list of targets is enriched for transcripts directly bound by
668 ORB2.

669

670 **The ORE directs ORB2 binding to and repression of a luciferase reporter mRNA in S2**
671 **cells**

672 To validate the biological activity of the ORE identified by #ATS, we used a luciferase
673 reporter assay in Drosophila S2 cells to measure ORB2 binding and ORB2-mediated regulation.

674 In the assay, firefly luciferase (FLuc) reporters harboured six copies in their 3′UTR of either a
675 representative ORE (UUUUGUU) or a mutated ORE (UUAUCUC) (the reporter is schematized
676 in Figure 3c). Each of these reporters was individually expressed in S2 cells together with either
677 a control protein (GFP), full-length ORB2 protein, or an ORB2 protein lacking its RBD
678 (ORB2ΔRRM). An unregulated Renilla luciferase (RLuc) reporter was co-transfected with all
679 samples, allowing us to normalize FLuc mRNA and protein levels.
680 ORB2 RIP followed by RT-qPCR confirmed that the reporters carrying the wild-type
681 OREs, but not the mutant OREs, were enriched in ORB2 IPs, compared to IPs of the
682 ORB2ΔRRM protein (Figure 3d). Furthermore, significant ORB2-mediated repression of the
683 reporter was seen when ORB2 protein was expressed together with a reporter construct carrying
684 wild-type OREs (Figure 3e). When either the OREs were mutated or the RRMs were deleted, no
685 repression was observed (Figure 3e) despite the fact that ORB2ΔRRM protein was expressed at
686 higher levels than full-length ORB2 (Figure S4).
687 We also assessed whether the firefly luciferase open reading frame used in the reporters
688 might be enriched for *Drosophila melanogaster* rare codons and found that this is indeed the
689 case (Figure S5). Our data do not address whether rare codon-enrichment per se contributes to
690 binding and/or repression; this would require the use of a codon-optimized version of luciferase,
691 which is beyond the scope of this study.
692 Our data do, however, clearly show that ORB2 binds to OREs in an RBD-dependent
693 manner and that this binding is sufficient to confer repression on the reporter RNA. The
694 magnitude of repression we observed is similar to that previously reported for ORB2B in similar
695 reporter assays in S2 cells (STEPIEN *et al.* 2016).
696
697 **The C-terminal Zinc-binding ('ZZ') domain of ORB2/hCPEB2 but not ORB/hCPEB1**
698 **represses a luciferase reporter mRNA in S2 cells**
699 To identify domains of ORB2 necessary and sufficient for repression we used a luciferase
700 reporter tethering assay in S2 cells. We transfected a plasmid construct that would express a
701 protein containing the BIV-Tat RNA-binding domain fused to all or part of the ORB2 protein.
702 This fusion protein is recruited to six tandem repeats of the trans-activating response (TAR)
703 element (to which BIV-Tat binds) located in the 3′UTR of a co-transfected firefly luciferase
704 reporter (schematised in Figure 4a) (WAKIYAMA *et al.* 2012; LAVER *et al.* 2020a). Tethering of

705 full-length ORB2B protein produced a significant, two-fold repression relative to a tethered GFP
706 control (Figure 4b); the extent of repression was consistent with previously published data for
707 ORB2 in S2 cells (STEPIEN *et al.* 2016). Tethering of ORB2 protein did not affect steady-state
708 reporter RNA levels (Figure 4c).
709 To map regions of ORB2 that mediate repression, we fused the BIV-Tat domain to
710 fragments of the ORB2 protein and assessed whether any individual region was capable of
711 repressing luciferase expression. We divided the ORB2 protein into five regions: IDR1, the
712 polyQ region, IDR2, the RBD, and the ZZ domain (Figures 1a and 4b,c). There was no
713 significant effect on the expression of luciferase after tethering of IDR1, polyQ, IDR1+polyQ,
714 IDR2 or RBD (Figure 4b and see Figure S6A for western blot of expression of each fragment).
715 Only the ZZ domain conferred strong (~three-fold) repression (Figure 4b) despite being
716 expressed at a comparatively low level (Figure S6a). To determine whether the ZZ domain was
717 also necessary for repression, we tethered an ORB2 protein construct lacking the ZZ domain
718 (ORB2ΔZZ) to the luciferase reporter and found that it was unable to repress luciferase
719 expression, despite ORB2ΔZZ retaining the RBD and being expressed at higher levels than full-
720 length ORB2 (Figure 4b, Figure S6b). Because luciferase mRNA levels were not significantly
721 different from controls in either the ZZ sufficiency or the ZZ necessity experiments (Figure 4c,
722 ZZ and ORB2ΔZZ), ZZ domain mediated repression can be attributed largely to effects on
723 translation rather than RNA stability. We conclude that the ZZ domain of ORB2 is both
724 necessary and sufficient to confer translational repression when tethered to a reporter mRNA.
725 Finally, to assess possible conservation of function, we also tethered the ZZ domains of
726 ORB, hCPEB1 and hCPEB2. The hCPEB2 ZZ domain conferred significant repression, whereas
727 the ORB ZZ and hCPEB1 ZZ domain were unable to repress (Figure 4e; western blot is shown
728 in Figure S6c). We conclude that the repressive function of the ZZ domain is conserved between
729 ORB2 and its human ortholog, hCPEB2, while it is not conserved in the more distantly related
730 proteins, ORB or hCPEB1. We note that the ZZ domains of hCPEB3 and hCPEB4 are ≥ 90%
731 identical to the hCPEB2 ZZ domain (Figure S7a). This suggests that, although not tested here,
732 the hCPEB3 and hCPEB4 ZZ domains likely also function in translational repression.
733
734 **Regions within the ORB2 ZZ domain function in combination to confer repression**

735 To map regions of the ORB2 ZZ domain sufficient for repression, we first compared the
736 sequences of the ZZ domains of ORB, ORB2, hCPEB1 and hCPEB2 (Figures 4d and S7a).
737 There is high level of sequence identity between the ORB2 ZZ domain and that of hCPEB2
738 (81.3% amino acid identity). In contrast, the ZZ domain of ORB2 and ORB, exhibit only 35.6%
739 sequence identity and hCPEB1 has only 28.5% amino acid identity to ORB2. We then
740 considered the predicted structures of these domains (Figure S8). An NMR structure of the
741 hCPEB1 ZZ domain showed it consists of a rubredoxin (Rd) turn, followed by a beta hairpin,
742 and a short alpha helix (MERKEL *et al.* 2013). Predictions of the structures of the ORB, ORB2
743 and hCPEB2 ZZ domains using Alphafold 3 (ABRAMSON *et al.* 2024) showed a similar
744 arrangement. Indeed, Alphafold3 prediction of the ORB ZZ structure was virtually identical to
745 that of the NMR structure of the hCPEB1 ZZ domain (Figure S8a). Similarly, the predictions of
746 the ORB2 and hCPEB2 ZZ structures were very similar to one another (Figure S8a). Finally, an
747 overlap of the ORB and ORB2 ZZ domain structures showed that the only difference was the
748 length of the Rd turn (Figure S8b).
749 To map regions within the ORB2 ZZ domain sufficient for repression we assessed whether
750 or not chimeric versions that included one or more of the Rd turn ('A', Q640 to P656), the beta
751 hairpin ('B', F657-Y668), the alpha helix ('C', C669 to Y684) and/or the C-terminal region ('D',
752 H685 to C-terminus) regions of the ORB or ORB2 ZZ domain functioned to repress firefly
753 luciferase expression using the tethering assay.
754 As expected, the full-length ORB2 ZZ domain repressed whereas the ORB ZZ domain did
755 not. Of the 14 chimeras tested, three resulted in significant repression relative to the GFP control
756 (Figure 4f, western blots are shown in Figure S7b,c): ORB2 ZZ-$A^1B^2C^2D^2$, ORB ZZ-$A^2B^1C^2D^1$
757 and ORB ZZ-$A^1B^1C^2D^2$ (where the superscript '2' refers to ORB2-derived sequences and
758 superscript '1' refers to ORB-derived sequences). The region shared by all of these mosaics is
759 ORB2 region C (denoted C^2), suggesting that it is a major contributor to the repressive function
760 of the ORB2 ZZ domain. However, ORB2 region C alone is not sufficient to confer repression
761 but needs to be combined with another ORB2 region (either A^2, B^2 or D^2) for repression.
762
763 **ORB2 interacts with translational repressors and the 43S translation preinitiation complex**
764 **in early embryos**

765 We next turned to proteomic strategies to identify protein partners of ORB2 in early
766 embryos. We immunoprecipitated endogenous ORB2 from extracts prepared from embryos
767 produced by w^{1118} females, both in the presence and absence of RNase A, in biological
768 quadruplicates, using the same synthetic antibody used above to identify ORB2 target RNAs.
769 Co-purifying proteins were identified by mass spectrometry followed by Significance Analysis
770 of INTeractome (SAINT), which assigns confidence scores to protein-protein interactions based
771 on comparisons between the Gaussian curves produced by the control IP data and the bait IP data
772 (CHOI *et al.* 2012). SAINT was performed with stringent parameters, where for each protein, the
773 lowest control and the highest bait were dropped prior to statistical analysis, which helped ensure
774 that only high-confidence interactors would be identified. We defined a protein interactor of
775 ORB2 as any protein that was significantly enriched in ORB2 immunoprecipitates compared to
776 parallel purifications using our negative control antibody, C1, with a SAINT (AvgP) score ≥
777 0.95 and a BFDR < 0.01 (File S4).
778 We identified 106 interactors in the presence of RNase A (Figures 5a and S10a),
779 representing RNA-independent interactions, and 212 interactors of ORB2 in the absence of
780 RNase A (Figure S10c,d); 85 were in common (File S4). The interactors largely fell into two
781 distinct groups: The first consisted of RBPs known to negatively regulate target stability and/or
782 translation, including AGO1, AGO2, PUM, and RBFOX1, as well as the Cup repressive
783 complex (Cup, ME31B, TRAL, BEL) (GOTZE *et al.* 2017) (Figure 5a,c File S4). All components
784 of the Cup repressive complex copurified in the presence of RNase (Figure 5a,c), consistent with
785 an RNA-independent interaction with ORB2. The second group consisted of translation-
786 initiation factors, notably the components of the 43S preinitiation complex (PIC): all eIF3 and
787 eIF2 subunits, eIF1 and -1A, and eIF5A; most (13/20) were RNA-independent interactors,
788 including 11/14 detected eIF3 subunits (Figure 5a,d and File S4).
789 We note that several of ORB2's protein interactors were also identified as mRNA targets
790 in our RIP-seq experiments (File S5). This result is consistent with an earlier study of RBP
791 mRNA targets and protein interactors carried out in S2 cells, which showed that RNP complexes
792 are enriched for both mRNAs and their encoded proteins involved in RNA binding and post-
793 transcriptional regulation (STOIBER *et al.* 2015).

794 Co-purification of ORB2 with post-transcriptional negative regulators is consistent with
795 our analyses of the post-transcriptional fate of ORB2 targets during the MZT and our reporter
796 experiments in S2 cells.
797
798 **The ORB2 ZZ domain is required for interaction with the 43S PIC and the Cup repressive**
799 **complex**
800 Our S2-cell tethering assay, described above, showed that the ZZ domain of ORB2 is
801 necessary and sufficient for translational repression; therefore, we assessed whether this domain
802 is important for association with ORB2's identified binding partners in early embryos. To
803 generate an endogenous deletion of the ZZ domain, we used a scarless dsRed CRISPR method to
804 remove all amino acids from ORB2 between D638 and the C-terminus at C704, inclusive,
805 leaving the endogenous 3′UTR intact (see Figure 4d, Materials and Methods, Figures S1, S2)
806 (GRATZ *et al.* 2013; GRATZ *et al.* 2014). The mutant fly lines resulting from the excision will
807 henceforth be referred to as *orb2*$^{\Delta ZZ}$. Western blots on whole-fly extract showed that ORB2ΔZZ
808 was expressed at higher levels than full-length ORB2 in the pre-CRISPRed *w*^{1118} wild-type
809 control flies (Figure S1d) and a similar result was obtained for 0-3 hour embryos (Figure S9a).
810 We confirmed by RIP-RT-qPCR that deletion of the ZZ domain did not significantly affect
811 ORB2ΔZZ's ability to bind to several of its RNA targets in embryos (Figure S9b). As assayed by
812 DAPI staining, *orb2*$^{\Delta ZZ}$ females showed no overt oogenesis defects; females outcrossed to the
813 control, host strain used for CRISPR produced embryos that underwent normal syncytial nuclear
814 cycles, cellularization and gastrulation, and exhibited similar hatch rates into first instar larvae as
815 the control (control: 92.5%. n = 200; *orb2*$^{\Delta ZZ}$: 90.7%, n = 300). We report elsewhere that *orb2*$^{\Delta ZZ}$
816 mutants have defects in brain development (HAILSTOCK *et al.* 2025) and spermatogenesis (LOW
817 *et al.* 2025).
818 Immunopurification of ORB2ΔZZ protein from 0-3-hour embryos produced by *orb2*$^{\Delta ZZ}$
819 homozygous females (henceforth referred to as *orb2*$^{\Delta ZZ}$ embryos) followed by mass spectrometry
820 identified 48 high-confidence protein interactors in the presence (Figure 5b, S10b) and 91 in the
821 absence of RNase A (Figure S10f), of which 43 overlapped (File S4). When the union of these
822 interactors (96 proteins) was compared to the union of full-length ORB2 IP-MS interactors (233
823 proteins), we found that 65 overlapped, including several translational repressors such as PUM
824 and RBFOX1 (Figure 5b, File S4). Strikingly, interactions with all components of the PIC and

825 the Cup repressive complex were lost upon deletion of the ZZ domain (compare Figure 5a and
826 5b).
827 We conclude that the ORB2 ZZ domain is required for interaction between ORB2 and the
828 43S PIC as well as the Cup repressive complex, but that additional repressors retain interaction
829 with ORB2 in the absence of its ZZ domain.
830
831 **Deletion of the ZZ domain results in a shift of ORB2 targets onto polysomes in the early**
832 **embryo**
833 Since our experiments in S2 cells showed that the ZZ domain is necessary for ORB2-
834 mediated translational repression, and our IP-MS results indicated that ORB2 loses interactions
835 with the Cup repressive complex when the ZZ domain is deleted, we next asked whether deletion
836 of the ZZ domain had consequences for post-transcriptional regulation of ORB2's target mRNAs
837 during the MZT. Notably, since embryos from *orb2*$^{\Delta ZZ}$ females undergo normal development and
838 binding to targets is unaffected by loss of the ZZ domain, any alterations in the post-
839 transcriptional fate of targets are likely to be a direct effect of the domain deletion rather than a
840 secondary consequence of abnormal development.
841 First, we assessed whether ORB2's targets, which are enriched for maternal transcripts that
842 are deadenylated and degraded during the MZT (see Figure 2e,f), were stabilized in *orb2*$^{\Delta ZZ}$
843 mutant embryos. We collected extracts from embryos laid by control or *orb2*$^{\Delta ZZ}$ females at 0-1,
844 1-2 and 2-3 hours after egg lay and carried out RNA-seq followed by analysis using DEseq2. We
845 compared the expression level of targets and co-expressed non-targets across this time course
846 and found that, at all three stages, there was no significant difference in expression level between
847 control versus ORB2ΔZZ embryos for either target or non-target transcripts (Figure 6a and File
848 S7). These results suggest that, while ORB2 binds to unstable mRNAs, it does not induce their
849 degradation or, alternatively, that ORB2 may direct destabilization of its targets during the MZT
850 in a ZZ domain-independent mechanism.
851 Second, we assessed whether ORB2's targets, which are enriched for transcripts with
852 significantly lower TE and TI than co-expressed non-targets (see Figure 2a-d), underwent an
853 increase in polysome association in ORB2ΔZZ embryos. We collected embryo extracts from
854 embryos laid by control or *orb2*$^{\Delta ZZ}$ females at 0-1, 1-2 and 2-3 hours after egg lay, then ran
855 polysome gradients followed by RNA-seq of pooled polysome fractions and pooled 'free' (non-

856 polysome-associated) fractions. For each gene, we calculated the ratio of RNA in the polysome
857 fractions to that in the free fractions (see Materials and Methods); if translational repression were
858 relieved upon deletion of the ZZ domain then this ratio would increase (i.e., transcripts would
859 move onto polysomes). We found that, in ORB2ΔZZ embryos, ORB2 targets shifted onto
860 polysomes at the first timepoint (0-1 hour) whereas non-targets did not (Figure 6b and File S7).
861 These data are consistent with the hypothesis that the ZZ domain of ORB2 mediates
862 translational repression of ORB2 targets early in the MZT, prior to ZGA. We note that we have
863 not directly demonstrated an increase in protein synthesis from these target transcripts in
864 embryos; however our S2 cell experiments showed that the ZZ domain is both necessary and
865 sufficient to repress luciferase protein expression without a change in reporter RNA levels,
866 consistent with the ZZ domain acting in translational repression.
867
868 **Co-regulation of ORB2 target transcripts by additional RBPs**
869 Although the shift onto polysomes of ORB2 targets at 0-1 hours in ORB2ΔZZ embryos
870 versus wild type is statistically significant ($P < 0.006$), it is subtle. We, therefore, decided to
871 assess whether ORB2 might function together with other post-transcriptional regulators known
872 to act during the MZT.
873 First, we asked whether there was a significant overlap of ORB2's targets with the targets
874 of several RBPs that we had analyzed previously. We found that ORB2 targets were depleted for
875 targets of Rasputin (RIN), an RBP that positively regulates transcript stability and translation
876 during the MZT (Table 5) (LAVER *et al.* 2020a), consistent with a role for ORB2 in negative
877 rather than positive regulation of its targets. In contrast, ORB2 targets significantly overlapped
878 those of PUM, BRAT and SMG (Table 5), RBPs that direct mRNA repression/degradation
879 during the MZT (TADROS *et al.* 2007; CHEN *et al.* 2014; LAVER *et al.* 2015).
880 For each of PUM, BRAT and SMG, we subdivided ORB2's targets into ones bound only
881 by ORB2, ones bound by both ORB2 and that RBP, ones bound only by that RBP, and co-
882 expressed unbound transcripts (see Materials and Methods, File S8). We found that, upon loss of
883 the ZZ domain, ORB2 targets bound by ORB2 but not SMG exhibited a significant shift onto
884 polysomes ($P = 0.009$; Figure 7b 'ORB2 only') whereas those co-bound by SMG (Figure 7a),
885 bound by SMG but not ORB2 (Figure 7c) or bound by neither ORB2 nor SMG (Figure 7d) did
886 not significantly shift onto polysomes. This result is consistent with the hypothesis that co-

887 regulation of a subset of ORB2's targets by SMG maintains repression (i.e., they do not shift
888 onto polysomes when the ZZ domain is deleted) and explains at least in part the subtle albeit
889 significant shift seen when ORB2 targets are aggregated (Figure 6b). Consistent with the SMG
890 analyses, ORB2 targets co-regulated (or not) by BRAT and PUM, exhibited a similar trend but
891 with the ORB2-only targets just missing significance (P = 0.062 and 0.073 for the PUM and
892 BRAT comparisons, respectively; Figures S11 and S12).
893 These data are consistent with the hypothesis that a significant subset of ORB2's targets
894 are coregulated by additional repressive RBPs, which attenuate the effect of loss of ORB2
895 repression upon deletion of the ZZ domain.
896
897 **DISCUSSION**
898 In this study, we identified hundreds of RNA targets and protein partners of the Drosophila
899 ORB2 protein in the early embryo. ORB2's targets are enriched for translationally repressed
900 mRNAs that are degraded during the MZT. ORB2-target open reading frames are enriched for
901 rare codons and a U-rich motif in their 3′UTR, the latter of which directs binding and repression
902 of a reporter in S2 cells. Repression by ORB2 is mediated by the ZZ domain, a function that is
903 conserved in hCPEB2. Deletion of the ZZ domain from the endogenous ORB2 gene results in
904 loss of physical interaction with the Cup repressive complex and movement of ORB2's mRNA
905 targets onto polysomes in the early embryo. Subsets of ORB2's targets are co-bound and likely
906 co-regulated by SMG.
907
908 **A conserved role for the ORB2/hCPEB2 ZZ domain in mediating translational repression**
909 Structural analysis of the ZZ domain of hCPEB1 has implicated it in protein-protein
910 interaction (MERKEL *et al.* 2013; STEPIEN *et al.* 2016), consistent with earlier studies on, for
911 example, the ZZ domain of CREB-binding protein (LEGGE *et al.* 2004). Our identification of
912 multiple proteins that depend *in vivo* on the ZZ domain for interaction with ORB2 are consistent
913 with a major role in recruiting co-regulators to target transcripts. Our data showing that deletion
914 of the ZZ domain does not affect RNA binding are consistent with a previous study (STEPIEN *et*
915 *al.* 2016). The fact that, in our S2 cell tethering assay, the ZZ domain is necessary and sufficient
916 for repression permitted us to assess evolutionary conservation of this role as well as to map
917 regions of the ZZ domain that implement this function.

918 Interestingly, we found that the repressive function of the entire ZZ domain is conserved
919 between ORB2 and hCPEB2 but not with ORB and hCPEB1. Chimeras containing regions from
920 the ORB2 and ORB ZZ domain showed that the α-helix (region C, C669 to H685) of ORB2 can
921 convert the ORB ZZ domain into a repressor when paired with one of the following: ORB2's Rd
922 turn at the N-terminus (Region A, Q640 to P656), the beta hairpin (Region B, F657-Y668), or
923 the C-terminal beta-sheet region (Region D, H685 to C-terminus). The ZZ domains of hCPEB3
924 and 4 show ≥ 90% amino acid identity to hCPEB2, with 16/17 residues of region A, 14/15 of
925 region B, 12/13 of region C, and 15/20 of D identical between hCPEB2-4. As such, it is quite
926 likely that the ZZ domains of hCPEB3 and 4 are also capable of repressing target mRNA
927 translation via region C.
928 That fact that region C of ORB2's ZZ domain needs one of A, B or D to convert the ORB
929 ZZ domain into a translational repressor is consistent with a model in which A, B or D bind
930 different co-repressors, any of which cooperate with C to mediate repression, or a model in
931 which A, B or D establish a structural context for C to interact with co-repressor(s). Future work
932 aimed at identifying the ORB2 binding partners that interact with each of regions A-D should
933 provide insights into the molecular mechanisms that underlie ZZ domain function.
934
935 **Regulation of post-transcriptional processes by ORB2 during the MZT: features of ORB2's**
936 **targets and their implications**
937 Three features in ORB2's target transcripts have implications for post-transcriptional
938 regulation during the MZT: enrichment for OREs, enrichment for rare codons, and enrichment
939 for binding sites for additional RBPs (notably SMG, BRAT and PUM).
940 First, enrichment for OREs and our evidence from S2 cell reporter assays that ORB2 binds
941 to OREs, which then confers repression on the reporter, are consistent with previous studies of
942 the binding specificity of ORB2 and ORB2B's role as a repressor (KHAN *et al.* 2015; STEPIEN *et*
943 *al.* 2016). Notably, since ORB2B is the only isoform expressed during the MZT, we conclude
944 that the *orb2* gene's function during the MZT is exclusively negative, which contrasts with its
945 role in other tissues. For example, in the nervous system, ORB2A and ORB2B are co-expressed,
946 permitting hetero-oligomer formation and translational upregulation of ORB2 targets
947 (MAJUMDAR *et al.* 2012; KHAN *et al.* 2015). Thus, expression specifically of the ORB2B isoform
948 during the MZT is a mechanism to negatively regulate the post-transcriptional fate of its targets.

949 Second, enrichment of ORB2's targets for rare codons is consistent with previous
950 observations in neurons, where it has been shown that ORB2 binds rare-codon enriched
951 transcripts (STEWART *et al.* 2024). In contrast to neurons, where the outcome is upregulation of
952 transcript stability and translation, embryonic targets of ORB2 are repressed and degraded. As
953 discussed above, this may be in part due to an absence of ORB2A and a consequence of only
954 having ORB2B present, but it may also be because of additional specific, negative-regulatory co-
955 factors that interact with ORB2 and/or ORB2 targets in embryos, as discussed in the next
956 section. Either way, the observation that ORB2 targets are enriched for rare codons and are
957 downregulated is consistent with the larger literature on the outcome of non-optimal codon
958 usage, including during the MZT of flies and vertebrates (PRESNYAK *et al.* 2015; BAZZINI *et al.*
959 2016; IRIARTE *et al.* 2021).
960 Third, we have shown that significant subsets of ORB2's targets are co-bound during the
961 MZT by SMG, BRAT and PUM. Our analyses of the ORB2 targets that move onto polysomes
962 when the ZZ domain is deleted are consistent with the hypothesis that co-regulated targets (e.g.,
963 those bound by both ORB2 and SMG) continue to be repressed, likely because SMG directs
964 ongoing repression, whereas ORB2-targets not bound by SMG shift onto polysomes. Whether
965 the latter are co-bound by additional unidentified RBPs is not yet known, but the fact that they
966 move onto polysomes suggests that, even if co-bound by such RBPs, those RBPs are not
967 sufficient for repression, at least not at the level of translation initiation.
968
969 **Regulation of post-transcriptional processes by ORB2 during the MZT: the role of**
970 **repressive co-factors**
971 Our analyses of the post-transcriptional fate of ORB2's targets during the MZT indicate
972 that they are enriched for transcripts that are translationally repressed and degraded. Consistent
973 with this outcome, multiple co-factors that are known to mediate repression and degradation of
974 mRNAs copurify with ORB2 in early embryos; most of these copurify in the presence of RNase,
975 consistent with an RNA-independent interaction with ORB2. Several of the regulators that
976 interact in an RNA-independent manner require the ZZ domain for interaction, notably the Cup
977 complex components Cup, TRAL, ME31B and BEL.
978 We have shown that the ZZ domain is necessary and sufficient for translational repression
979 of reporters in S2 cells and deletion of the ZZ domain results in a shift of ORB2's *in vivo* targets

980 onto polysomes in 0-1-hour embryos. That the Cup complex is expressed in both S2 cells and
981 embryos, that ZZ domain deletion results in loss of Cup complex interaction with ORB2 in
982 embryos, and that ORB2's targets in embryos move onto polysomes when the ZZ domain is
983 deleted from endogenous ORB2, are all consistent with the hypothesis that ORB2-dependent
984 repression is mediated by the Cup complex. The Cup complex prevents interaction of eIF4G
985 with eIF4E, thus abrogating translation initiation (WILHELM *et al.* 2003; NAKAMURA *et al.* 2004;
986 NELSON *et al.* 2004a); consistent with this role, we note that, while eIF4E was present in our
987 ORB2 IP-MS data, eIF4G was absent. Previous studies have shown that the Cup complex is
988 brought to mRNAs by BRU or Squid (SQD) in oocytes and by SMG in embryos (WILHELM *et al.*
989 2003; NAKAMURA *et al.* 2004; NELSON *et al.* 2004a; CLOUSE *et al.* 2008). ORB2, thus, represents
990 a second RBP that acts in embryos to recruit this complex for repression, in this case early in the
991 MZT. A caveat is that we have not demonstrated that the targets that shift onto polysomes are
992 translated; post-initiation mechanisms may act to prevent protein synthesis.
993 The Cup complex has been shown to be cleared by the CTLH E3 ligase part-way through
994 the MZT (CAO *et al.* 2020; ZAVORTINK *et al.* 2020), consistent with the ZZ domain's repressive
995 role in the early but not late MZT. However, ORB2's targets are repressed at both 0-1 hours
996 (when the Cup complex is present) and at 2-3 hours (after the Cup complex has been cleared);
997 furthermore, ORB2's targets are deadenylated and degraded between 0-1 and 2-3 hours, but
998 deletion of the ZZ domain has no effect on their clearance. These data suggest that additional
999 regulators may function either independent of or together with ORB2 to direct these processes.
1000 SMG is an example of a co-regulator present throughout the MZT that acts through the Cup
1001 complex for repression and through the CCR4-NOT deadenylase to direct degradation (NELSON
1002 *et al.* 2004b; SEMOTOK *et al.* 2005). SMG's co-purification with ORB2 in our IP-MS
1003 experiments is RNA-dependent; thus, SMG's binding and regulation of a subset of ORB2-targets
1004 may be independent of physical interaction with ORB2. PUM, FMR1 and RBFOX1 are also
1005 present throughout the MZT (CASAS-VILA *et al.* 2017; CAO *et al.* 2020) and we have shown here
1006 that their interaction with ORB2 is both RNA-independent and ZZ-domain independent, making
1007 them candidates for implementing these roles together with ORB2 but independent of its ZZ
1008 domain.
1009
1010 **The mystery of PIC interaction**

1011 Unexpectedly, we identified the 43S PIC as a major interactor of ORB2 via its ZZ domain.
1012 An essential component of the PIC is the eIF3 complex (its subunits are encoded by 14 genes in
1013 *Drosophila*), which is a highly regulated component of translation initiation (HARRIS *et al.* 2006;
1014 CHIU *et al.* 2010; CATE 2017). Several of the mammalian eIF3 subunits have been shown to have
1015 RNA-binding ability (LEE *et al.* 2015; LEE *et al.* 2016) and to mediate distinct regulatory
1016 outcomes (PESTOVA *et al.* 1998; PESTOVA AND HELLEN 1999; HUI *et al.* 2003; HUI *et al.* 2005;
1017 MARTINEAU *et al.* 2008; LEE *et al.* 2010; MARTINEAU *et al.* 2014).
1018 At this time we do not have data that provide insights into the functional consequences of
1019 ORB2's interaction with the PIC. ORB2's interaction with the PIC's eIF3 subunits is RNA-
1020 independent, consistent with direct interaction with one or more of these subunits. We
1021 considered one possibile mechanism where ORB2 may sequester the PIC, thus limiting its
1022 availability and reducing translation overall. However, in such a model, one would expect a
1023 global increase in translation upon loss of PIC interaction rather than what we observed in
1024 *orb2*$^{\Delta ZZ}$ embryos, which is an increase in polysome association of ORB2's targets but no change
1025 in non-targets. An alternative hypothesis is that ORB2-dependent binding to the PIC on target
1026 transcripts has a negative effect on translation, either in addition to or in concert with the Cup
1027 repressive complex. Indeed, a speculative model might be that ORB2 binding to the 3′UTR and
1028 its interaction with PIC at the 5′UTR might repress translation initiation by interfering with PIC
1029 function or enhancing the function of repressive elements of the eIF3 complex. The mechanistic
1030 and functional consequences of ORB2-PIC interaction will be a fruitful area for future study.
1031

1032 **Data Availability**

1033 Drosophila strains are available upon request. Raw data for RIP-seq, RNA-seq and IP-MS
1034 are available at GEO (GSE299661 for RIP-seq, GSE299140 for RNA-seq time-course,
1035 GSE299019 for polysome gradient seq) and at MassIVE (MSV000098275 for IP-MS). The
1036 authors affirm that all of the other data necessary for confirming the conclusions of the article are
1037 present within the article, figures, tables and supplementary files.
1038

1039 **Acknowledgements**

We thank Kun Nie for assisting with the *de novo* motif discovery using #ATS, Dr. Dorothy Lerit and Dr. Donald Fox for feedback on draft and preprint versions of this manuscript, respectively.

Funding

This research was supported by grants from the Canadian Institutes of Health Research PJT-159702 (HDL), PJT-190124 (HDL) and PJT-159494 (CAS). TCHL was supported in part by a Canada Graduate Scholarship (CGS-M) and a University of Toronto Open Fellowship; CW and ZW were supported in part by University of Toronto Open Fellowships. Molecular graphics and analyses were performed with UCSF ChimeraX, developed by the Resource for Biocomputing, Visualization, and Informatics at the University of California, San Francisco, with support from National Institutes of Health R01-GM129325 and the Office of Cyber Infrastructure and Computational Biology, National Institute of Allergy and Infectious Diseases.

Conflicts of Interest

The authors declare that they have no conflicts of interest.

1056 **LITERATURE CITED**

1057

1058 Abramson, J., J. Adler, J. Dunger, R. Evans, T. Green *et al.*, 2024 Accurate structure prediction
1059 of biomolecular interactions with AlphaFold 3. Nature 630**:** 493-500.
1060 Bazzini, A. A., F. Del Viso, M. A. Moreno-Mateos, T. G. Johnstone, C. E. Vejnar *et al.*, 2016
1061 Codon identity regulates mRNA stability and translation efficiency during the maternal-
1062 to-zygotic transition. EMBO J 35**:** 2087-2103.
1063 Bernhart, S. H., I. L. Hofacker and P. F. Stadler, 2006 Local RNA base pairing probabilities in
1064 large sequences. Bioinformatics 22**:** 614-615.
1065 Cao, W. X., S. Kabelitz, M. Gupta, E. Yeung, S. Lin *et al.*, 2020 Precise Temporal Regulation of
1066 Post-transcriptional Repressors Is Required for an Orderly Drosophila Maternal-to-
1067 Zygotic Transition. Cell Rep 31**:** 107783.
1068 Casas-Vila, N., A. Bluhm, S. Sayols, N. Dinges, M. Dejung *et al.*, 2017 The developmental
1069 proteome of Drosophila melanogaster. Genome Res 27**:** 1273-1285.
1070 Cate, J. H., 2017 Human eIF3: from 'blobology' to biological insight. Philos Trans R Soc Lond B
1071 Biol Sci 372.
1072 Chen, L., J. G. Dumelie, X. Li, M. H. Cheng, Z. Yang *et al.*, 2014 Global regulation of mRNA
1073 translation and stability in the early Drosophila embryo by the Smaug RNA-binding
1074 protein. Genome Biol 15**:** R4.
1075 Chiu, C. W. N., C. Monat, M. Robitaille, M. Lacomme, A. M. Daulat *et al.*, 2016 SAPCD2
1076 Controls Spindle Orientation and Asymmetric Divisions by Negatively Regulating the
1077 Galphai-LGN-NuMA Ternary Complex. Dev Cell 36**:** 50-62.
1078 Chiu, W. L., S. Wagner, A. Herrmannová, L. Burela, F. Zhang *et al.*, 2010 The C-terminal
1079 region of eukaryotic translation initiation factor 3a (eIF3a) promotes mRNA recruitment,
1080 scanning, and, together with eIF3j and the eIF3b RNA recognition motif, selection of
1081 AUG start codons. Mol Cell Biol 30**:** 4415-4434.
1082 Choi, H., G. Liu, D. Mellacheruvu, M. Tyers, A. C. Gingras *et al.*, 2012 Analyzing protein-
1083 protein interactions from affinity purification-mass spectrometry data with SAINT. Curr
1084 Protoc Bioinformatics Chapter 8**:** Unit8.15.
1085 Clouse, K. N., S. B. Ferguson and T. Schupbach, 2008 Squid, Cup, and PABP55B function
1086 together to regulate gurken translation in Drosophila. Dev Biol 313**:** 713-724.
1087 de Moor, C. H., and J. D. Richter, 1999 Cytoplasmic polyadenylation elements mediate masking
1088 and unmasking of cyclin B1 mRNA. EMBO J 18**:** 2294-2303.
1089 De Renzis, S., O. Elemento, S. Tavazoie and E. F. Wieschaus, 2007 Unmasking activation of the
1090 zygotic genome using chromosomal deletions in the Drosophila embryo. PLoS Biol 5**:**
1091 e117.
1092 Dunn, J. G., C. K. Foo, N. G. Belletier, E. R. Gavis and J. S. Weissman, 2013 Ribosome
1093 profiling reveals pervasive and regulated stop codon readthrough in Drosophila
1094 melanogaster. Elife 2**:** e01179.
1095 Duran-Arqué, B., M. Cañete, C. L. Castellazzi, A. Bartomeu, A. Ferrer-Caelles *et al.*, 2022
1096 Comparative analyses of vertebrate CPEB proteins define two subfamilies with
1097 coordinated yet distinct functions in post-transcriptional gene regulation. Genome Biol
1098 23**:** 192.

1099 Eichhorn, S. W., A. O. Subtelny, I. Kronja, J. C. Kwasnieski, T. L. Orr-Weaver *et al.*, 2016
1100 mRNA poly(A)-tail changes specified by deadenylation broadly reshape translation in
1101 Drosophila oocytes and early embryos. Elife 5.
1102 Fernández-Miranda, G., and R. Méndez, 2012 The CPEB-family of proteins, translational
1103 control in senescence and cancer. Ageing Res Rev 11**:** 460-472.
1104 Franz, M., H. Rodriguez, C. Lopes, K. Zuberi, J. Montojo *et al.*, 2018 GeneMANIA update
1105 2018. Nucleic Acids Res 46**:** W60-W64.
1106 Gene Ontology, C., S. A. Aleksander, J. Balhoff, S. Carbon, J. M. Cherry *et al.*, 2023 The Gene
1107 Ontology knowledgebase in 2023. Genetics 224.
1108 Gilmutdinov, R., E. N. Kozlov, K. V. Yakovlev, L. V. Olenina, A. A. Kotov *et al.*, 2021 The
1109 3'UTR of the Drosophila CPEB translation factor gene orb2 plays a crucial role in
1110 spermatogenesis. Development 148.
1111 Gotze, M., J. Dufourt, C. Ihling, C. Rammelt, S. Pierson *et al.*, 2017 Translational repression of
1112 the Drosophila nanos mRNA involves the RNA helicase Belle and RNA coating by
1113 Me31B and Trailer hitch. RNA 23**:** 1552-1568.
1114 Gratz, S. J., A. M. Cummings, J. N. Nguyen, D. C. Hamm, L. K. Donohue *et al.*, 2013 Genome
1115 engineering of Drosophila with the CRISPR RNA-guided Cas9 nuclease. Genetics 194**:**
1116 1029-1035.
1117 Gratz, S. J., F. P. Ukken, C. D. Rubinstein, G. Thiede, L. K. Donohue *et al.*, 2014 Highly
1118 specific and efficient CRISPR/Cas9-catalyzed homology-directed repair in Drosophila.
1119 Genetics 196**:** 961-971.
1120 Groisman, I., Y. S. Huang, R. Mendez, Q. Cao and J. D. Richter, 2001 Translational control of
1121 embryonic cell division by CPEB and maskin. Cold Spring Harb Symp Quant Biol 66**:**
1122 345-351.
1123 Hafer, N., S. Xu, K. M. Bhat and P. Schedl, 2011 The Drosophila CPEB protein Orb2 has a
1124 novel expression pattern and is important for asymmetric cell division and nervous
1125 system function. Genetics 189**:** 907-921.
1126 Hailstock, T., J. Buehler, B. V. Robinson, T. C. H. Low, Y. Hua *et al.*, 2025 The CPEB ortholog
1127 Orb2 regulates brain size through the TRIM-NHL RNA-binding protein, Brain tumor.
1128 bioRxiv.
1129 Hake, L. E., and J. D. Richter, 1994 CPEB is a specificity factor that mediates cytoplasmic
1130 polyadenylation during Xenopus oocyte maturation. Cell 79**:** 617-627.
1131 Harris, T. E., A. Chi, J. Shabanowitz, D. F. Hunt, R. E. Rhoads *et al.*, 2006 mTOR-dependent
1132 stimulation of the association of eIF4G and eIF3 by insulin. EMBO J 25**:** 1659-1668.
1133 Harrison, M. M., A. J. Marsh and C. A. Rushlow, 2023 Setting the stage for development: the
1134 maternal-to-zygotic transition in Drosophila. Genetics 225.
1135 Haugen, R. J., C. Barnier, N. D. Elrod, H. Luo, M. K. Jensen *et al.*, 2024 Regulation of the
1136 Drosophila transcriptome by Pumilio and the CCR4-NOT deadenylase complex. RNA
1137 30**:** 866-890.
1138 Hervás, R., L. Li, A. Majumdar, M. e. C. Fernández-Ramírez, J. R. Unruh *et al.*, 2016 Molecular
1139 Basis of Orb2 Amyloidogenesis and Blockade of Memory Consolidation. PLoS Biol 14**:**
1140 e1002361.
1141 Hervas, R., M. J. Rau, Y. Park, W. Zhang, A. G. Murzin *et al.*, 2020 Cryo-EM structure of a
1142 neuronal functional amyloid implicated in memory persistence in *Drosophila*. Science
1143 367**:** 1230-1234.

1144 Hui, D. J., C. R. Bhasker, W. C. Merrick and G. C. Sen, 2003 Viral stress-inducible protein p56
1145 inhibits translation by blocking the interaction of eIF3 with the ternary complex
1146 eIF2.GTP.Met-tRNAi. J Biol Chem 278**:** 39477-39482.
1147 Hui, D. J., F. Terenzi, W. C. Merrick and G. C. Sen, 2005 Mouse p56 blocks a distinct function
1148 of eukaryotic initiation factor 3 in translation initiation. J Biol Chem 280**:** 3433-3440.
1149 Iriarte, A., G. Lamolle and H. Musto, 2021 Codon Usage Bias: An Endless Tale. J Mol Evol 89**:**
1150 589-593.
1151 Ivshina, M., P. Lasko and J. D. Richter, 2014 Cytoplasmic polyadenylation element binding
1152 proteins in development, health, and disease. Annu Rev Cell Dev Biol 30**:** 393-415.
1153 Jiang, T., R. F. McKinley, M. A. McGill, S. Angers and T. J. Harris, 2015 A Par-1-Par-3-
1154 Centrosome Cell Polarity Pathway and Its Tuning for Isotropic Cell Adhesion. Curr Biol
1155 25**:** 2701-2708.
1156 Jumper, J., R. Evans, A. Pritzel, T. Green, M. Figurnov *et al.*, 2021 Applying and improving
1157 AlphaFold at CASP14. Proteins 89**:** 1711-1721.
1158 Keleman, K., S. Krüttner, M. Alenius and B. J. Dickson, 2007 Function of the Drosophila CPEB
1159 protein Orb2 in long-term courtship memory. Nat Neurosci 10**:** 1587-1593.
1160 Khan, M. R., L. Li, C. Pérez-Sánchez, A. Saraf, L. Florens *et al.*, 2015 Amyloidogenic
1161 Oligomerization Transforms Drosophila Orb2 from a Translation Repressor to an
1162 Activator. Cell 163**:** 1468-1483.
1163 Kim, J. H., and J. D. Richter, 2006 Opposing polymerase-deadenylase activities regulate
1164 cytoplasmic polyadenylation. Mol Cell 24**:** 173-183.
1165 Kolberg, L., U. Raudvere, I. Kuzmin, P. Adler, J. Vilo *et al.*, 2023 g:Profiler-interoperable web
1166 service for functional enrichment analysis and gene identifier mapping (2023 update).
1167 Nucleic Acids Res 51**:** W207-W212.
1168 Kopylova, E., L. Noe and H. Touzet, 2012 SortMeRNA: fast and accurate filtering of ribosomal
1169 RNAs in metatranscriptomic data. Bioinformatics 28**:** 3211-3217.
1170 Kozlov, E., Y. V. Shidlovskii, R. Gilmutdinov, P. Schedl and M. Zhukova, 2021 The role of
1171 CPEB family proteins in the nervous system function in the norm and pathology. Cell
1172 Biosci 11**:** 64.
1173 Kozlov, E. N., E. V. Tokmatcheva, A. M. Khrustaleva, E. S. Grebenshchikov, R. V. Deev *et al.*,
1174 2023 Long-Term Memory Formation in Drosophila Depends on the 3'UTR of CPEB
1175 Gene orb2. Cells 12.
1176 Kronja, I., B. Yuan, S. W. Eichhorn, K. Dzeyk, J. Krijgsveld *et al.*, 2014 Widespread changes in
1177 the posttranscriptional landscape at the Drosophila oocyte-to-embryo transition. Cell Rep
1178 7**:** 1495-1508.
1179 Krüttner, S., B. Stepien, J. N. Noordermeer, M. A. Mommaas, K. Mechtler *et al.*, 2012
1180 Drosophila CPEB Orb2A mediates memory independent of Its RNA-binding domain.
1181 Neuron 76**:** 383-395.
1182 Laver, J. D., K. Ancevicius, P. Sollazzo, J. T. Westwood, S. S. Sidhu *et al.*, 2012 Synthetic
1183 antibodies as tools to probe RNA-binding protein function. Mol Biosyst 8**:** 1650-1657.
1184 Laver, J. D., X. Li, D. Ray, K. B. Cook, N. A. Hahn *et al.*, 2015 Brain tumor is a sequence-
1185 specific RNA-binding protein that directs maternal mRNA clearance during the
1186 Drosophila maternal-to-zygotic transition. Genome Biol 16**:** 94.
1187 Laver, J. D., J. Ly, A. K. Winn, A. Karaiskakis, S. Lin *et al.*, 2020a The RNA-Binding Protein
1188 Rasputin/G3BP Enhances the Stability and Translation of Its Target mRNAs. Cell Rep
1189 30**:** 3353-3367.e3357.

1190 Laver, J. D., J. Ly, A. K. Winn, A. Karaiskakis, S. Lin *et al.*, 2020b The RNA-Binding Protein
1191 Rasputin/G3BP Enhances the Stability and Translation of Its Target mRNAs. Cell Rep
1192 30**:** 3353-3367 e3357.
1193 Lécuyer, E., H. Yoshida, N. Parthasarathy, C. Alm, T. Babak *et al.*, 2007 Global analysis of
1194 mRNA localization reveals a prominent role in organizing cellular architecture and
1195 function. Cell 131**:** 174-187.
1196 Lee, A. S., P. J. Kranzusch and J. H. Cate, 2015 eIF3 targets cell-proliferation messenger RNAs
1197 for translational activation or repression. Nature 522**:** 111-114.
1198 Lee, A. S., P. J. Kranzusch, J. A. Doudna and J. H. Cate, 2016 eIF3d is an mRNA cap-binding
1199 protein that is required for specialized translation initiation. Nature 536**:** 96-99.
1200 Lee, J. P., A. Brauweiler, M. Rudolph, J. E. Hooper, H. A. Drabkin *et al.*, 2010 The TRC8
1201 ubiquitin ligase is sterol regulated and interacts with lipid and protein biosynthetic
1202 pathways. Mol Cancer Res 8**:** 93-106.
1203 Legge, G. B., M. A. Martinez-Yamout, D. M. Hambly, T. Trinh, B. M. Lee *et al.*, 2004 ZZ
1204 domain of CBP: an unusual zinc finger fold in a protein interaction module. J Mol Biol
1205 343**:** 1081-1093.
1206 Li, X., G. Quon, H. D. Lipshitz and Q. Morris, 2010 Predicting in vivo binding sites of RNA-
1207 binding proteins using mRNA secondary structure. RNA 16**:** 1096-1107.
1208 Liu, G., J. Zhang, H. Choi, J. P. Lambert, T. Srikumar *et al.*, 2012 Using ProHits to store,
1209 annotate, and analyze affinity purification-mass spectrometry (AP-MS) data. Curr Protoc
1210 Bioinformatics Chapter 8**:** 8.16.11-18.16.32.
1211 Liu, G., J. Zhang, B. Larsen, C. Stark, A. Breitkreutz *et al.*, 2010 ProHits: integrated software for
1212 mass spectrometry-based interaction proteomics. Nat Biotechnol 28**:** 1015-1017.
1213 Liu, Y. C., A. L. Couzens, A. R. Deshwar, B. M.-C. LD, X. Zhang *et al.*, 2014 The PPFIA1-
1214 PP2A protein complex promotes trafficking of Kif7 to the ciliary tip and Hedgehog
1215 signaling. Sci Signal 7**:** ra117.
1216 Lorenz, R., S. H. Bernhart, C. Honer Zu Siederdissen, H. Tafer, C. Flamm *et al.*, 2011
1217 ViennaRNA Package 2.0. Algorithms Mol Biol 6**:** 26.
1218 Love, M. I., W. Huber and S. Anders, 2014 Moderated estimation of fold change and dispersion
1219 for RNA-seq data with DESeq2. Genome Biol 15**:** 550.
1220 Love, M. I., C. Soneson, P. F. Hickey, L. K. Johnson, N. T. Pierce *et al.*, 2020 Tximeta:
1221 Reference sequence checksums for provenance identification in RNA-seq. PLoS Comput
1222 Biol 16**:** e1007664.
1223 Low, T. C. H., B. L. Falk, J. A. Brill and H. D. Lipshitz, 2025 The C-terminal ZZ domain of the
1224 Drosophila ORB2 RNA-binding protein is required for spermatid individualization.
1225 bioRxiv**:** 2025.2008.2022.671863.
1226 Majumdar, A., W. C. Cesario, E. White-Grindley, H. Jiang, F. Ren *et al.*, 2012 Critical role of
1227 amyloid-like oligomers of Drosophila Orb2 in the persistence of memory. Cell 148**:** 515-
1228 529.
1229 Martineau, Y., M. C. Derry, X. Wang, A. Yanagiya, J. J. Berlanga *et al.*, 2008 Poly(A)-binding
1230 protein-interacting protein 1 binds to eukaryotic translation initiation factor 3 to stimulate
1231 translation. Mol Cell Biol 28**:** 6658-6667.
1232 Martineau, Y., X. Wang, T. Alain, E. Petroulakis, D. Shahbazian *et al.*, 2014 Control of Paip1-
1233 eukayrotic translation initiation factor 3 interaction by amino acids through S6 kinase.
1234 Mol Cell Biol 34**:** 1046-1053.

1235 Mastushita-Sakai, T., E. White-Grindley, J. Samuelson, C. Seidel and K. Si, 2010 Drosophila
1236 Orb2 targets genes involved in neuronal growth, synapse formation, and protein turnover.
1237 Proc Natl Acad Sci U S A 107**:** 11987-11992.
1238 Meng, E. C., T. D. Goddard, E. F. Pettersen, G. S. Couch, Z. J. Pearson *et al.*, 2023 UCSF
1239 ChimeraX: Tools for structure building and analysis. Protein Sci 32**:** e4792.
1240 Merkel, D. J., S. B. Wells, B. C. Hilburn, F. Elazzouzi, G. C. Pérez-Alvarado *et al.*, 2013 The C-
1241 terminal region of cytoplasmic polyadenylation element binding protein is a ZZ domain
1242 with potential for protein-protein interactions. J Mol Biol 425**:** 2015-2026.
1243 Montojo, J., K. Zuberi, H. Rodriguez, F. Kazi, G. Wright *et al.*, 2010 GeneMANIA Cytoscape
1244 plugin: fast gene function predictions on the desktop. Bioinformatics 26**:** 2927-2928.
1245 Na, H., J. D. Laver, J. Jeon, F. Singh, K. Ancevicius *et al.*, 2016 A high-throughput pipeline for
1246 the production of synthetic antibodies for analysis of ribonucleoprotein complexes. RNA
1247 22**:** 636-655.
1248 Nakamura, A., K. Sato and K. Hanyu-Nakamura, 2004 Drosophila cup is an eIF4E binding
1249 protein that associates with Bruno and regulates oskar mRNA translation in oogenesis.
1250 Dev Cell 6**:** 69-78.
1251 Nakamura, Y., T. Gojobori and T. Ikemura, 2000 Codon usage tabulated from international
1252 DNA sequence databases: status for the year 2000. Nucleic Acids Res 28**:** 292.
1253 Nelson, M. R., A. M. Leidal and C. A. Smibert, 2004a Drosophila Cup is an eIF4E-binding
1254 protein that functions in Smaug-mediated translational repression. The EMBO journal
1255 23**:** 150-159.
1256 Nelson, M. R., A. M. Leidal and C. A. Smibert, 2004b Drosophila Cup is an eIF4E-binding
1257 protein that functions in Smaug-mediated translational repression. EMBO J 23**:** 150-159.
1258 Ozturk-Colak, A., S. J. Marygold, G. Antonazzo, H. Attrill, D. Goutte-Gattat *et al.*, 2024
1259 FlyBase: updates to the Drosophila genes and genomes database. Genetics 227.
1260 Patro, R., G. Duggal, M. I. Love, R. A. Irizarry and C. Kingsford, 2017 Salmon provides fast and
1261 bias-aware quantification of transcript expression. Nat Methods 14**:** 417-419.
1262 Pestova, T. V., and C. U. Hellen, 1999 Internal initiation of translation of bovine viral diarrhea
1263 virus RNA. Virology 258**:** 249-256.
1264 Pestova, T. V., I. N. Shatsky, S. P. Fletcher, R. J. Jackson and C. U. Hellen, 1998 A prokaryotic-
1265 like mode of cytoplasmic eukaryotic ribosome binding to the initiation codon during
1266 internal translation initiation of hepatitis C and classical swine fever virus RNAs. Genes
1267 Dev 12**:** 67-83.
1268 Presnyak, V., N. Alhusaini, Y. H. Chen, S. Martin, N. Morris *et al.*, 2015 Codon optimality is a
1269 major determinant of mRNA stability. Cell 160**:** 1111-1124.
1270 Puigbo, P., I. G. Bravo and S. Garcia-Vallve, 2008 CAIcal: a combined set of tools to assess
1271 codon usage adaptation. Biol Direct 3**:** 38.
1272 Ray, D., H. Kazan, K. B. Cook, M. T. Weirauch, H. S. Najafabadi *et al.*, 2013 A compendium of
1273 RNA-binding motifs for decoding gene regulation. Nature 499**:** 172-177.
1274 Semotok, J. L., R. L. Cooperstock, B. D. Pinder, H. K. Vari, H. D. Lipshitz *et al.*, 2005 Smaug
1275 recruits the CCR4/POP2/NOT deadenylase complex to trigger maternal transcript
1276 localization in the early Drosophila embryo. Curr Biol 15**:** 284-294.
1277 Shannon, P., A. Markiel, O. Ozier, N. S. Baliga, J. T. Wang *et al.*, 2003 Cytoscape: a software
1278 environment for integrated models of biomolecular interaction networks. Genome Res
1279 13**:** 2498-2504.

1280 Standart, N., and N. Minshall, 2008 Translational control in early development: CPEB, P-bodies
1281 and germinal granules. Biochem Soc Trans 36**:** 671-676.
1282 Stepien, B. K., C. Oppitz, D. Gerlach, U. Dag, M. Novatchkova *et al.*, 2016 RNA-binding
1283 profiles of Drosophila CPEB proteins Orb and Orb2. Proc Natl Acad Sci U S A 113**:**
1284 E7030-E7038.
1285 Stewart, R. K., P. Nguyen, A. Laederach, P. C. Volkan, J. K. Sawyer *et al.*, 2024 Orb2 enables
1286 rare-codon-enriched mRNA expression during Drosophila neuron differentiation. Nat
1287 Commun 15**:** 5270.
1288 Stoiber, M. H., S. Olson, G. E. May, M. O. Duff, J. Manent *et al.*, 2015 Extensive cross-
1289 regulation of post-transcriptional regulatory networks in Drosophila. Genome Res 25**:**
1290 1692-1702.
1291 Supek, F., and K. Vlahovicek, 2005 Comparison of codon usage measures and their applicability
1292 in prediction of microbial gene expressivity. BMC Bioinformatics 6**:** 182.
1293 Tadros, W., A. L. Goldman, T. Babak, F. Menzies, L. Vardy *et al.*, 2007 SMAUG is a major
1294 regulator of maternal mRNA destabilization in Drosophila and its translation is activated
1295 by the PAN GU kinase. Dev Cell 12**:** 143-155.
1296 Tadros, W., and H. D. Lipshitz, 2009 The maternal-to-zygotic transition: a play in two acts.
1297 Development 136**:** 3033-3042.
1298 Thomsen, S., S. Anders, S. C. Janga, W. Huber and C. R. Alonso, 2010 Genome-wide analysis
1299 of mRNA decay patterns during early Drosophila development. Genome Biol 11**:** R93.
1300 Vastenhouw, N. L., W. X. Cao and H. D. Lipshitz, 2019 The maternal-to-zygotic transition
1301 revisited. Development 146.
1302 Wakiyama, M., Y. Kaitsu, R. Muramatsu, K. Takimoto and S. Yokoyama, 2012 Tethering of
1303 proteins to RNAs using the bovine immunodeficiency virus-Tat peptide and BIV-TAR
1304 RNA. Anal Biochem 427**:** 130-132.
1305 Wang, X. P., and N. G. Cooper, 2009 Characterization of the transcripts and protein isoforms for
1306 cytoplasmic polyadenylation element binding protein-3 (CPEB3) in the mouse retina.
1307 BMC Mol Biol 10**:** 109.
1308 Warde-Farley, D., S. L. Donaldson, O. Comes, K. Zuberi, R. Badrawi *et al.*, 2010 The
1309 GeneMANIA prediction server: biological network integration for gene prioritization and
1310 predicting gene function. Nucleic Acids Res 38**:** W214-220.
1311 Whitten, D., 2011 Classification and clustering of sequencing data using a Poisson model, pp.
1312 2493-2518. Annals of Applied Statistics.
1313 Wilhelm, J. E., M. Hilton, Q. Amos and W. J. Henzel, 2003 Cup is an eIF4E binding protein
1314 required for both the translational repression of oskar and the recruitment of Barentsz. J
1315 Cell Biol 163**:** 1197-1204.
1316 Xu, S., N. Hafer, B. Agunwamba and P. Schedl, 2012 The CPEB protein Orb2 has multiple
1317 functions during spermatogenesis in Drosophila melanogaster. PLoS Genet 8**:** e1003079.
1318 Zavortink, M., L. N. Rutt, S. Dzitoyeva, J. C. Henriksen, C. Barrington *et al.*, 2020 The E2
1319 Marie Kondo and the CTLH E3 ligase clear deposited RNA binding proteins during the
1320 maternal-to-zygotic transition. Elife 9.

1321

1322 ## Figure Legends

1323 **Figure 1. RIP-seq identifies over 450 ORB2 targets in 0-3 hr embryos.** (a) Domain structure
1324 of ORB2B and location of the antigen used to screen for phage-displayed synthetic antibodies.
1325 (b) Scatterplot depicting the Log_2(Fold Enrichment compared to Input) for all genes identified in
1326 the RIP-seq analysis; each point represents a single gene. Values represent the average
1327 enrichment from three independent biological replicates. ORB2 targets (red) are defined as
1328 having fold enrichment > 1.5 in the anti-ORB2 RIP-seq compared to input and a ratio of
1329 ORB2/Control > 1.5, with an FDR adjusted *P*-value < 0.05; genes enriched in both ORB2 and
1330 control RIP-seq (green) are defined as having fold enrichment > 1.5 in both anti-ORB2 and
1331 control RIP-seq, with a ratio of ORB2/Control < 1.5 and an FDR adjusted *P*-value < 0.05;
1332 Control enriched transcripts (blue) are defined as having fold enrichment < -1.5 in the control
1333 RIP-seq, fold enrichment < -1.5 in the anti-ORB2 RIP-seq, and an FDR adjusted *P*-value < 0.05.
1334 Dotted lines indicate ±1.5 fold-change thresholds. (c) Violin and boxplots depicting the
1335 distribution of transcript abundance as measured by average TPM from three biological
1336 replicates based on target status as described in (A). Wilcoxon Rank Sum Test with Bonferroni
1337 multiple-test correction: ** = $P < 10^{-10}$; *** = $P < 10^{-15}$. (d) Validation of RIP-seq targets by RT-
1338 qPCR; bar graphs depict the log_2(fold enrichment) in an anti-ORB2 RIP-RT-qPCR compared to
1339 control RIP-RT-qPCR; *P*-values given are derived from Wilcoxon Signed Rank Test comparing
1340 ORB2 RIP-RT-qPCR to control RIP-RT-qPCR.

1341 **Figure 2. ORB2 target transcripts are enriched in translationally repressed, unstable, rare-**
1342 **codon containing transcripts during the MZT.** Violin plots and boxplots depicting the
1343 relationship between ORB2-association and translational status, change in poly(A) tail length,
1344 and change in transcript abundance. Non-target genes include all expressed genes that were not
1345 defined as ORB2 targets in the RIP-seq analysis. (a) Translation efficiency, calculated from
1346 ribosome footprinting performed on 0-1 hour embryo extracts (EICHHORN *et al.* 2016). (b)
1347 Translation efficiency, calculated from ribosome footprinting performed on 2-3 hour embryo
1348 extracts (EICHHORN *et al.* 2016). (c) Translation efficiency as measured by ribosome profiling
1349 performed on 0-2 hour embryo extracts (DUNN *et al.* 2013). (d) Translation index, calculated
1350 from polysome gradients performed on 0-3 hour embryo extracts (CHEN *et al.* 2014). (e) Change
1351 in transcript poly(A) tail length, calculated by comparing 0-1 hour and 2-3 hour embryo extracts,
1352 as measured by PAL-Seq (EICHHORN *et al.* 2016). (f) Change in abundance, calculated by
1353 comparing 0-1 hour and 2-3 hour embryo extracts, as measured by RNA-Seq (EICHHORN *et al.*
1354 2016). (g) MELP score, calculated for all annotated CDS longer than 80 codons on FlyBase 6.58
1355 by coRdon with ribosomal proteins as the references for codon optimization, and the isoform
1356 with minimum score (the worst expressivity) is chosen to represent each expressed gene. (h) CAI
1357 score, calculated for all annotated CDS longer than 80 codons on FlyBase 6.58 by local version
1358 of CAIcal with the *Drosophila melanogaster* codon usage table from the Kazusa codon usage
1359 database, and the isoform with minimum score (the most enriched for rare codons) is chosen to
1360 represent each expressed gene. Wilcoxon Rank Sum Test: ** = $P < 10^{-10}$; *** = $P < 10^{-15}$.

1361 **Figure 3. ORB2 binding motifs predicted from RIP-seq confer translational repression on a**
1362 **reporter mRNA in S2 cells.** (a) The #ATS *de novo* motif discovery program (LI *et al.* 2010)
1363 was performed on the results from the anti-ORB2 RIP-seq in this study. #ATS identified
1364 NUUGUWU as the ORB2 recognition element (ORE) enriched in ORB2 targets. (b) The
1365 transcriptome was evaluated for accessible enrichment of the NUUGUWU motif and each

1366 transcript was scored based on the number and accessibility of these motif sites. ORB2 targets
1367 had significantly higher scores compared to non-targets, as assessed by Wilcoxon rank sum test.
1368 *** = $P < 10^{-15}$ (c) Diagram depicting the reporter firefly luciferase mRNA with six copies of
1369 different ORB2-binding motifs in the 3′UTR. (d) Bar graph depicting the enrichment of the
1370 luciferase reporter mRNA in an anti-ORB2 RIP-qPCR compared to Renilla luciferase mRNA,
1371 normalized to a reporter without ORE motifs. Mutation of the OREs or deletion of the RNA-
1372 binding domain (RRM) abrogate binding to the mRNA. (e) Bar graph depicting the ratio of
1373 luminescence between firefly luciferase and Renilla luciferase. Mutation of the OREs or deletion
1374 of the RNA-binding domain (RRM) abrogate repression. One-way Kruskal-Wallis non-
1375 parametric test with Dunn multiple test correction: * = $P < 0.05$.

1376 **Figure 4. The ORB2 and hCPEB2 ZZ domain but not the ORB and hCPEB1 ZZ domain**
1377 **repress a luciferase reporter. (**a) Diagram depicting the tethering assay in which a polypeptide
1378 of interest fused to the BIV-Tat domain is tethered to a firefly luciferase reporter mRNA carrying
1379 six tandem repeat TAR elements in the 3′UTR. (b) Bar graph depicting the expression of the
1380 reporter firefly luciferase (normalized to co-transfected Renilla luciferase and normalized to
1381 steady state RNA levels) when tethering whole ORB2 or ORB2 fragments compared to GFP
1382 control. (c) Bar graph depicting the expression of the reporter firefly luciferase mRNA measured
1383 by RT-qPCR (normalized to co-transfected Renilla luciferase mRNA) when tethering whole
1384 ORB2 or ORB2 fragments compared to GFP control. Reporter mRNA levels are unaffected by
1385 ORB2 ZZ or ORB2ΔZZ. (d) amino acid sequence alignment of the ZZ domains of ORB2, ORB,
1386 and their human orthologs, hCPEB1 and hCPEB2. The arrowhead denotes the junction between
1387 the RBD and ZZ domains. (e) Bar graph depicting the expression of the reporter firefly luciferase
1388 (normalized to co-transfected Renilla luciferase) when tethering different CPEB ZZ domains.
1389 Only ORB2 and hCPEB2 repress. (f) Bar graph depicting the expression of the reporter firefly
1390 luciferase when ORB ZZ chimeric domains harboring substitutions from the ORB2 ZZ domain,
1391 are tethered. One-way Kruskal-Wallis non-parametric test with Dunn multiple test correction: *
1392 = $P < 0.05$.

1393 **Figure 5. Anti-ORB2 IP-MS from early embryo extracts identifies known translation**
1394 **repressors and the PIC as binding partners.** (a-b) Scatterplots depicting all proteins identified
1395 in the IP-MS performed in the presence of RNase. Enrichment is expressed as the Log_2 ratio of
1396 the average spectral counts detected in the ORB2 IP compared to the average spectral counts
1397 detected in the control IP. Protein interactors were identified by SAINT (with a SAINT score ≥
1398 0.95 and BFDR < 0.01), shown in red. (a) IP-MS performed on embryos laid by w^{1118} females,
1399 (b) IP-MS performed on embryos laid by $orb2^{\Delta ZZ}$ females. (c) Interaction network depicting the
1400 connections between components of the Cup repressive complex and other translational
1401 repressors identified as ORB2 interactors by SAINT analysis. (d) Interaction network depicting
1402 the connections between components of eukaryotic PIC identified as ORB2 interactors by
1403 SAINT analysis. Interaction networks were produced by the GeneMANIA app for Cytoscape
1404 (FRANZ *et al.* 2018); size of node indicates average number of spectral counts obtained in the
1405 ORB2 IP-MS; thickness of edges indicates strength of interaction assigned by GeneMANIA.

1406 **Figure 6. Deletion of the ORB2 ZZ domain results in derepression of target RNAs in the**
1407 **early embryo.** (a) Violin and boxplots comparing target and non-target abundance as determined
1408 by RNA-Seq in 0-1, 1-2 and 2-3 hour old embryos laid by w^{1118} and $orb2^{\Delta ZZ}$ females. No
1409 significant difference was detected for either genotype at any of the time-points. (b) Violin plots

1410 and boxplots comparing target and non-target translation index as determined by polysome
1411 gradients followed by RNA-Seq in 0-1, 1-2 and 2-3 hour old embryos laid by w^{1118} and $orb2^{\Delta ZZ}$
1412 females. ORB2 targets were significantly derepressed in 0-1 hour old $orb2^{\Delta ZZ}$ embryos relative to
1413 w^{1118}. Log2(Ratio of mean normalized counts of pool 3/mean normalized counts of pool 1) was
1414 calculated for each transcript. Wilcoxon Rank Sum Test: ** = $P < 0.01$.

1415 **Figure 7. ORB2 targets which are co-bound by SMG are not repressed in the early embryo.**
1416 (a-d) Violin and boxplots comparing the polysome association of ORB2 and SMG co-targets (a),
1417 ORB2 targets (b), SMG targets (c), and non-targets (d), as determined by polysome gradients
1418 followed by RNA-Seq in 0-1 hour old embryos laid by w^{1118} control (WT) and $orb2^{\Delta ZZ}$ females.
1419 Wilcoxon Rank Sum Test ** = $P < 0.01$.

1420

1421 ## Table Legends

1422 **Table 1. Overlap between the list of ORB2 targets and lists of genes associated with mRNA**
1423 **stability or decay in the early embryo.**

1424 **Table 2. Molecular Function GO-terms enriched in ORB2 targets.** GO-term analysis was
1425 performed using the gProfiler2 tool (KOLBERG *et al.* 2023).

1426 **Table 3. Biological Process GO-terms enriched in ORB2 targets.** GO-term analysis was
1427 performed using the gProfiler2 tool (KOLBERG *et al.* 2023).

1428 **Table 4. Cellular Component GO-terms enriched in ORB2 targets.** GO-term analysis was
1429 performed using the gProfiler2 tool (KOLBERG *et al.* 2023).

1430 **Table 5. Overlap of ORB2 targets with those bound by SMG, BRAT, PUM and RIN.**

1431

1432 ## Supplemental Figure Legends

1433 **Figure S1. CRISPR Cas9-mediated endogenous deletion of the ORB2 ZZ domain was used**
1434 **to generate $orb2^{\Delta ZZ}$ flies.** (a) Diagram depicting the *orb2* endogenous locus, located at 66E4-
1435 66E5 on 3L, the corresponding mRNAs that are encoded, and the targeted deletion. (b) Agarose
1436 gel of the PCR amplification of the region surrounding the CRISPR targeted deletion of the F1
1437 generation post-injection. Genotypes indicate lines generated from individual F1 flies. Up PCR
1438 indicates PCR amplification using primers designed against the 5′ insertion junction; Down PCR
1439 indicates PCR amplification using primers designed against the 3′ insertion junction. (c) Agarose
1440 gel of the PCR amplification of the region surrounding the PiggyBac transposon-mediated
1441 excision of the dsRed marker. WT indicates the band representing PCR amplification of the
1442 endogenous ORB2 locus containing an intact ZZ domain; Excised indicates the band
1443 representing amplification of the locus with the ZZ domain deletion without the dsRed marker.
1444 Genotypes indicate lines generated from individual flies resulting from the CRISPR injection. (d)
1445 Western blot showing expression of endogenous ORB2 and CRISPRed ORB2ΔZZ in
1446 heterozygous and homozygous whole flies. ORB2ΔZZ is expressed at higher levels than full-

1447 length ORB2 (see heterozygote for comparison). Generation of CRISPR mutants was performed
1448 by WellGenetics as described in the Materials and Methods.

1449 **Figure S2. Sequence of the CRISPR Cas9-mediated endogenous deletion of the ORB2 ZZ**
1450 **domain.**

1451 **Figure S3. Replicate-to-replicate comparisons of transcript TPMs from RIP-seq**
1452 **experiments show high correlation between replicates.** (a)-(c) Pairwise comparisons of the
1453 three biological replicates performed with the anti-ORB2 E8 Fab. The Pearson correlation
1454 coefficient and its corresponding *P*-value were calculated and used to determine the degree of
1455 similarity between each pair. (d) Heatmap of the Poisson distance between three biological RIP-
1456 seq replicates performed with anti-ORB2 E8 Fab and three biological RIP-seq replicates
1457 performed with control C1 Fab. The Poisson distance is calculated by the difference in Poisson
1458 distribution between pairs of samples; a larger distance indicates a greater level of dissimilarity
1459 between samples.

1460 **Figure S4. Evaluation of RNA Compete motif enrichment and expression levels of ORB2,**
1461 **ORB2ΔRRM, and GFP in S2 cells.** (a) The transcriptome was evaluated for accessible
1462 enrichment of the KUUUKKK motif and each transcript was scored based on the number and
1463 accessibility of these motif sites, as in Figure 3b. ORB2 targets had significantly higher scores
1464 compared to non-targets, as assessed by Wilcoxon rank sum test. *** = $P < 10^{-15}$. (b) Each set of
1465 three lanes corresponds to the ORE validation experiments in which expression vectors for
1466 tagged proteins and reporter mRNA constructs containing various recognition motifs were
1467 transfected into S2 cells, described in Figure 3d and 3e.

1468 **Figure S5. The firefly luciferase open reading frame used in the FLuc reporter is enriched**
1469 **for rare codons.** (a) Distribution of CAI scores, calculated for all annotated CDS longer than 80
1470 codons on FlyBase 6.58 by local version of CAIcal with the *Drosophila melanogaster* codon
1471 usage table from the Kazusa codon usage database, and the isoform with minimum score (the
1472 most enriched for rare codons) is chosen to represent each expressed gene. (b) Distribution of
1473 MELP scores, calculated for all annotated CDS longer than 80 codons on FlyBase 6.58 by
1474 coRdon with ribosomal proteins as the references for codon optimization, and the isoform with
1475 minimum score (the worst expressivity) is chosen to represent each expressed gene. In (a) and
1476 (b) the scores for the firefly luciferase open reading frame are indicated by the dashed blue lines.

1477 **Figure S6. Expression of ORB2 full-length protein, portions of ORB2, and the ZZ domains**
1478 **of ORB, ORB2, hPCPEB1 and 2 in S2 cells.** (a) Western blot showing the expression of ORB2
1479 full-length protein and protein portions corresponding to the experiments described in Figure 4b
1480 and c. (b) Western blot showing the expression of ORB2B and ORB2BΔZZ to the experiments
1481 described in Figure 4b and c. (c) Western blot showing the expression of ORB2 ZZ, hCPEB2
1482 ZZ, ORB ZZ and hCPEB1 ZZ corresponding to the experiments described in Figure 4e.

1483 **Figure S7. Expression of chimeric ORB-ORB2 ZZ domain proteins in S2 cells.** (a)
1484 Schematic depicting the amino acid sequence alignment of the ZZ domains of ORB2, ORB, and
1485 their human orthologs, hCPEB1, hCPEB2, hCPEB3, and hCPEB4. The arrowhead denotes the
1486 junction between the RBD and ZZ domains. (b) Bar graph depicting the expression of the
1487 reporter firefly luciferase when ORB ZZ chimeric domains harboring substitutions from the

1488 ORB2 ZZ domain, are tethered. The ORB2 'A' and 'C' regions are each sufficient to convert the
1489 ORB ZZ domain into a repressor. One-way Kruskal-Wallis non-parametric test with Dunn
1490 multiple test correction was used to assess significance. (c) Western blot showing the expression
1491 of ORB-ORB2 chimeric proteins corresponding to the substitution experiments which assessed
1492 transformation of the non-repressing ORB ZZ domain into a translational repressor, as shown in
1493 S7b above.

1494 **Figure S8. Structure of ZZ domains of CPEB family members.** (a) The NMR structure of the
1495 ZZ domain of human CPEB1 Protein Data Bank accession 2M13 (MERKEL *et al.* 2013) is
1496 shown, along with the Alphafold 3 (ABRAMSON *et al.* 2024) predicted structures of the ZZ
1497 domains of ORB, hCPEB2 and ORB2. The colors in the Alphafold 3 predictions represent the
1498 predicted local distance difference test (pLDDT) scores, where higher numbers indicate greater
1499 confidence in the prediction. (b) On the left is an overlap of the ORB and ORB2 predicted
1500 structures with Region A (the Rd turn), Region B (the beta hairpin), Region C (the alpha helix),
1501 and Region D (the beta sheet) of each protein indicated. The boxes on the right depict the most
1502 confident structure within each region in two different orientations.

1503 **Figure S9. ORB2ΔZZ retains RNA-binding to its targets in embryos.** (a) Western blot
1504 showing the expression of ORB2 and ORB2ΔZZ protein over the first four hours of embryonic
1505 development. (b) Bar graph depicting the enrichment of five ORB2 target mRNAs in RIP-RT-
1506 qPCR from 0-3 hour old embryos laid by w^{1118} and $orb2^{\Delta ZZ}$ females. The ORB2 RIPs used the
1507 ORB2 E8 Fab; the control RIP used the C1 Fab. RNA levels were normalized to *RpL32* mRNA.
1508 n = 3; error bars are standard deviation. Student's *t*-test *P*-values were not significant (n.s.; $P >$
1509 0.05)

1510 **Figure S10. IP-MS identifies ORB2 protein interactors.** (a,b,d,e) Scatterplots depicting all
1511 proteins identified in the IP-MS. Log_2(average spectral counts) from the ORB2 IP is plotted
1512 against the Log_2(average spectral counts) from the control IP. (a) IP-MS performed on embryos
1513 laid by w^{1118} females in the presence of RNase (corresponding to Figure 5a), (b) IP-MS
1514 performed on embryos laid by $orb2^{\Delta ZZ}$ females in the presence of RNase (corresponding to
1515 Figure 5b), (d) IP-MS performed on embryos laid by w^{1118} females in the absence of RNase, and
1516 (e) IP-MS performed on embryos laid by $orb2^{\Delta ZZ}$ females in the absence of RNase. (c, d)
1517 Scatterplots depicting all proteins identified in the IP-MS performed in the absence of RNase.
1518 Enrichment is expressed as the Log_2 ratio of the average spectral counts detected in the ORB2 IP
1519 compared to the average spectral counts detected in the control IP. Protein interactors were
1520 identified by SAINT (with a SAINT score ≥ 0.95 and BFDR < 0.01), shown in red.

1521 **Figure S11. ORB2 targets which are co-bound by PUM are not de-repressed in the early**
1522 **embryo.** (a-d) Violin plots and boxplots comparing the translation index of ORB2 and PUM co-
1523 targets (a), ORB2 targets (b), PUM targets (c), and non-targets (d), as determined by polysome
1524 gradients followed by RNA-Seq in 0-1 hour old embryos laid by w^{1118} and $orb2^{\Delta ZZ}$ females.
1525 Wilcoxon Rank Sum Test *P*-values are shown.
1526

1527 **Figure S12. ORB2 targets which are co-bound by BRAT are not de-repressed in the early**
1528 **embryo.** (a-d) Violin plots and boxplots comparing the translation index of ORB2 and BRAT
1529 co-targets (a), ORB2 targets (b), BRAT targets (c), and non-targets (d), as determined by

1530 polysome gradients followed by RNA-Seq in 0-1 hour old embryos laid by w^{1118} and $orb^{2\Delta ZZ}$
1531 females. Wilcoxon Rank Sum Test *P*-values are shown.
1532

1533 Supplemental File Legends

1534 **File S1. Results of RIP-seq of ORB2 in 0-3 hour embryos.** See Materials and Methods for
1535 details.

1536 **File S2. Results of rare codon enrichment analyses on ORB2 targets in 0-3 hour embryos.**
1537 The MELP and CAI were calculated as described in Materials and Methods.

1538 **File S3. Results of *de novo* motif discovery on ORB2 targets in 0-3 hour embryos.** Motif
1539 discovery was carried out using #ATS as described (LI *et al.* 2010). ORE scores and
1540 'KUUUKKK' scores are listed. See Materials and Methods for details.

1541 **File S4. Results of IP-MS of ORB2 and ORB2ΔZZ in 0-3 hour embryos in the presence or**
1542 **absence of RNase A.** Interactors were identified using SAINT as described (CHOI *et al.* 2012).
1543 See Materials and Methods for details.

1544 **File S5. Lists of mRNAs bound by ORB2 (RIP-seq) whose protein products were also**
1545 **identified as interactors in ORB2 IP-MS.**

1546 **File S6. Results of RNA-seq time-course in wild-type and ORB2ΔZZ embryos.** See Materials
1547 and Methods for details.

1548 **File S7. Results of polysome gradient RNA-seq time-course in wild-type and ORB2ΔZZ**
1549 **embryos.** See Materials and Methods for details.

1550 **File S8. Overlaps of ORB2 targets and previously identified SMG, BRAT and PUM targets.**
1551 See Materials and Methods for details.

FIGURE 1

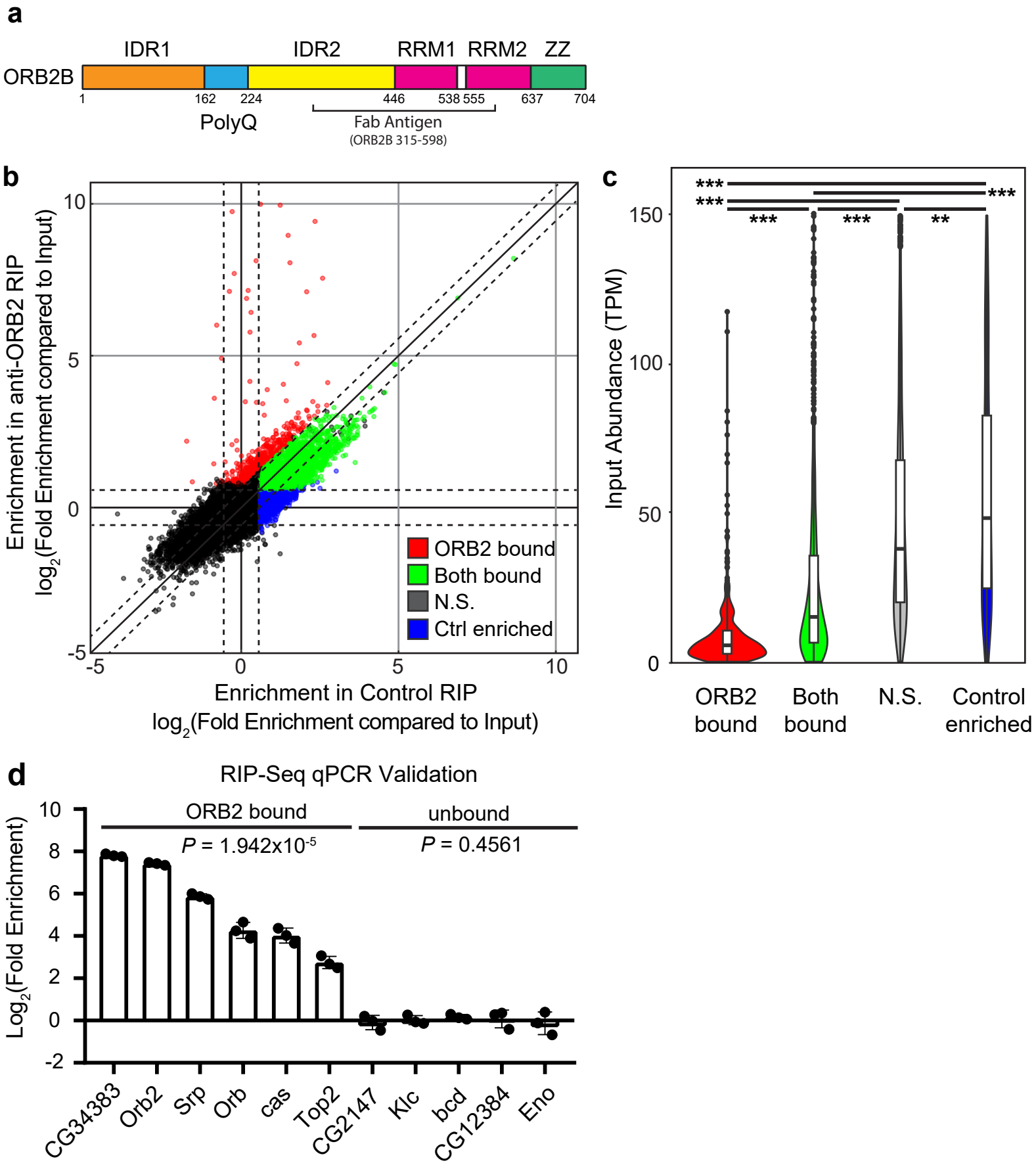
a
IDR1
IDR2
RRM1
RRM2
ZZ
ORB2B
1
162
224
446
538
555
637
704
PolyQ
Fab Antigen
(ORB2B 315-598)
b
Enrichment in anti-ORB2 RIP
log2(Fold Enrichment compared to Input)
Enrichment in Control RIP
log2(Fold Enrichment compared to Input)
ORB2 bound
Both bound
N.S.
Ctrl enriched
c
Input Abundance (TPM)
ORB2 bound
Both bound
N.S.
Control enriched
d
RIP-Seq qPCR Validation
ORB2 bound
unbound
P = 1.942x10-5
P = 0.4561
Log2(Fold Enrichment)
CG34383
Orb2
Srp
Orb
cas
Top2
CG2147
Klc
bcd
CG12384
Eno

FIGURE 2

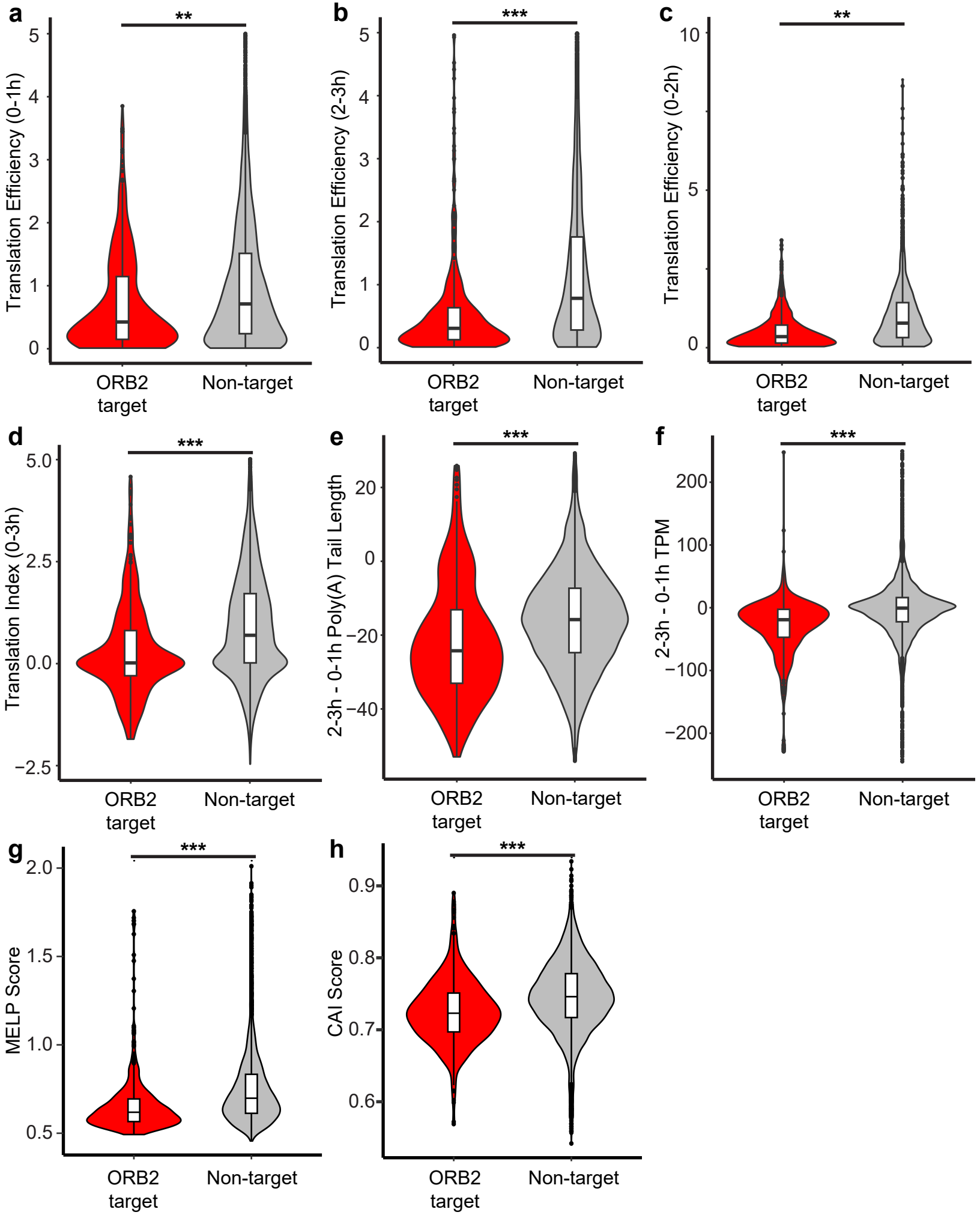
a
**
Translation Efficiency (0-1h)
0
1
2
3
4
5
ORB2 target
Non-target
b
***
Translation Efficiency (2-3h)
0
1
2
3
4
5
ORB2 target
Non-target
c
**
Translation Efficiency (0-2h)
0
5
10
ORB2 target
Non-target
d
***
Translation Index (0-3h)
−2.5
0.0
2.5
5.0
ORB2 target
Non-target
e
***
2-3h - 0-1h Poly(A) Tail Length
−40
−20
0
20
ORB2 target
Non-target
f
***
2-3h - 0-1h TPM
−200
−100
0
100
200
ORB2 target
Non-target
g
***
MELP Score
0.5
1.0
1.5
2.0
ORB2 target
Non-target
h
***
CAI Score
0.6
0.7
0.8
0.9
ORB2 target
Non-target

FIGURE 3

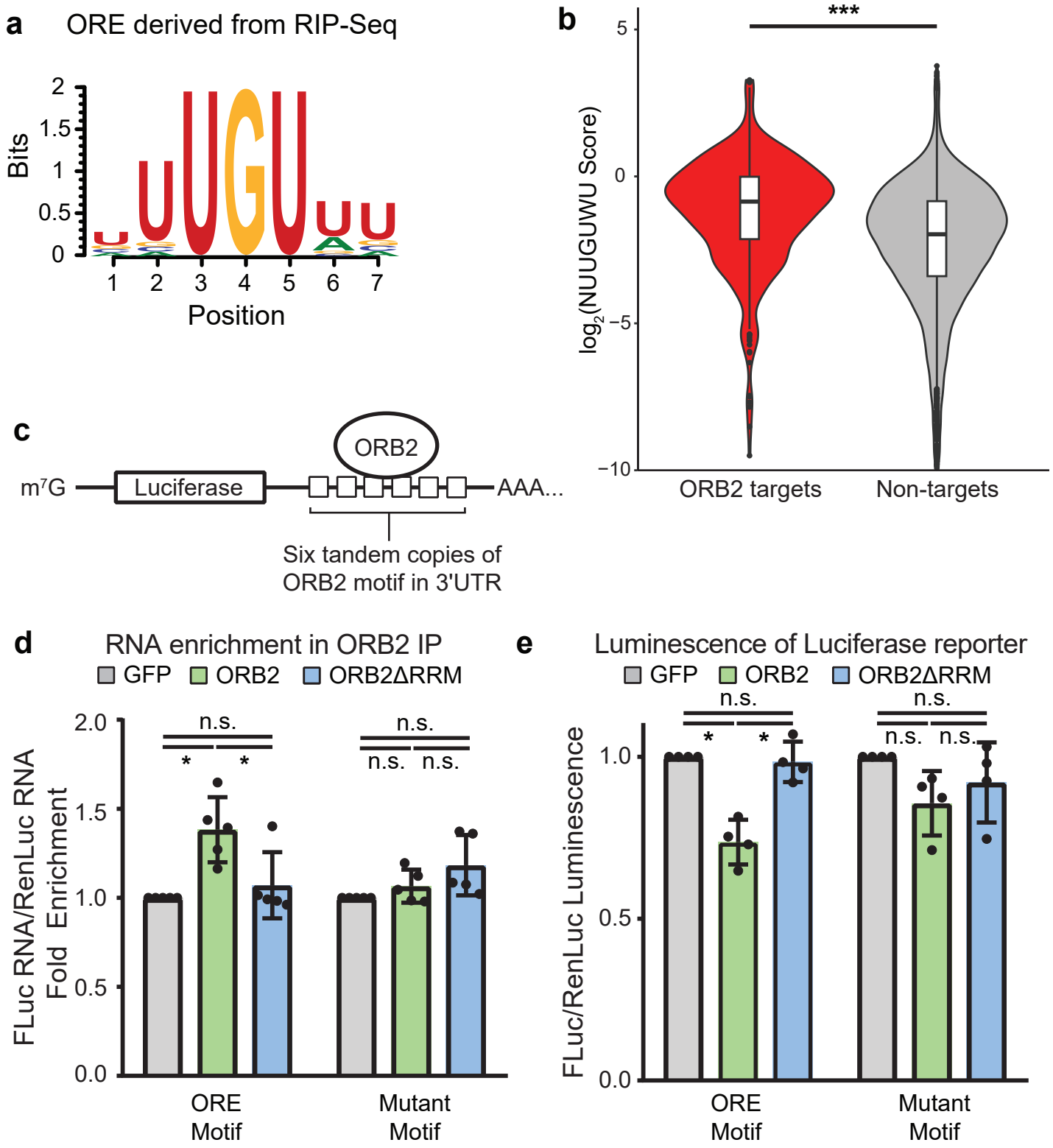
a
ORE derived from RIP-Seq
Bits
2
1.5
1
0.5
0
1 2 3 4 5 6 7
Position
b
***
5
0
−5
−10
log2(NUUGUWU Score)
ORB2 targets
Non-targets
c
ORB2
m7G
Luciferase
AAA...
Six tandem copies of
ORB2 motif in 3'UTR
d
RNA enrichment in ORB2 IP
GFP
ORB2
ORB2ΔRRM
n.s.
*
*
n.s.
n.s.
n.s.
2.0
1.5
1.0
0.5
0.0
FLuc RNA/RenLuc RNA
Fold Enrichment
ORE
Motif
Mutant
Motif
e
Luminescence of Luciferase reporter
GFP
ORB2
ORB2ΔRRM
n.s.
*
*
n.s.
n.s.
n.s.
1.0
0.5
0.0
FLuc/RenLuc Luminescence
ORE
Motif
Mutant
Motif

FIGURE 4

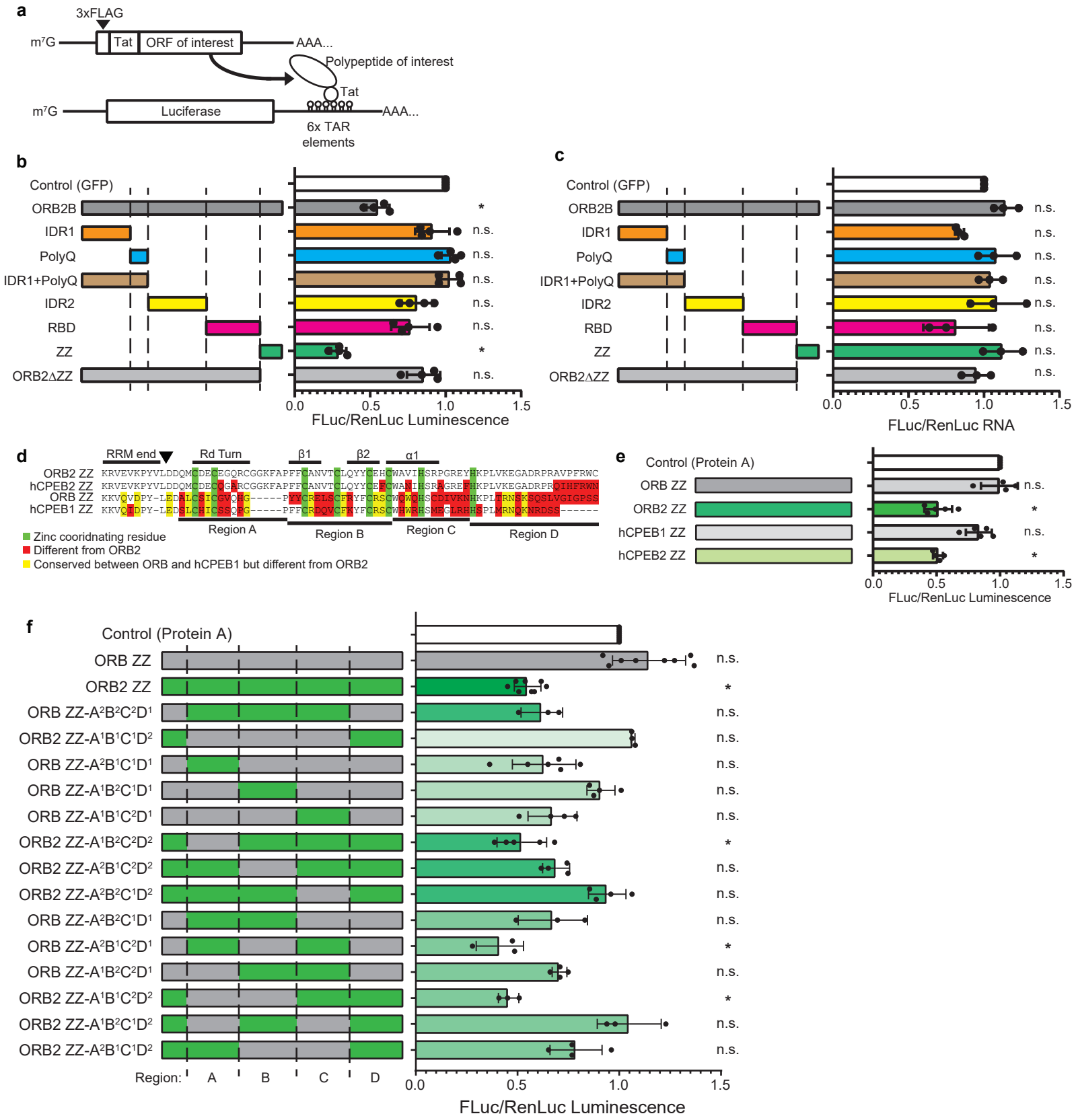
a
3xFLAG
m7G
Tat
ORF of interest
AAA...
Polypeptide of interest
Tat
m7G
Luciferase
AAA...
6x TAR elements
b
Control (GFP)
ORB2B
IDR1
PolyQ
IDR1+PolyQ
IDR2
RBD
ZZ
ORB2ΔZZ
*
n.s.
n.s.
n.s.
n.s.
n.s.
n.s.
*
n.s.
0.0
0.5
1.0
1.5
FLuc/RenLuc Luminescence
c
Control (GFP)
ORB2B
IDR1
PolyQ
IDR1+PolyQ
IDR2
RBD
ZZ
ORB2ΔZZ
n.s.
n.s.
n.s.
n.s.
n.s.
n.s.
n.s.
n.s.
n.s.
0.0
0.5
1.0
1.5
FLuc/RenLuc RNA
d
RRM end
Rd Turn
β1
β2
α1
ORB2 ZZ
hCPEB2 ZZ
ORB ZZ
hCPEB1 ZZ
Region A
Region B
Region C
Region D
Zinc cooridnating residue
Different from ORB2
Conserved between ORB and hCPEB1 but different from ORB2
e
Control (Protein A)
ORB ZZ
ORB2 ZZ
hCPEB1 ZZ
hCPEB2 ZZ
n.s.
*
n.s.
*
0.0
0.5
1.0
1.5
FLuc/RenLuc Luminescence
f
Control (Protein A)
ORB ZZ
ORB2 ZZ
ORB ZZ-A2B2C2D1
ORB2 ZZ-A1B1C1D2
ORB ZZ-A2B1C1D1
ORB ZZ-A1B2C1D1
ORB ZZ-A1B1C2D1
ORB2 ZZ-A1B2C2D2
ORB2 ZZ-A2B1C2D2
ORB2 ZZ-A2B2C1D2
ORB ZZ-A2B2C1D1
ORB ZZ-A2B1C2D1
ORB ZZ-A1B2C2D1
ORB2 ZZ-A1B1C2D2
ORB2 ZZ-A1B2C1D2
ORB2 ZZ-A2B1C1D2
n.s.
*
n.s.
n.s.
n.s.
n.s.
n.s.
*
n.s.
n.s.
n.s.
*
n.s.
*
n.s.
n.s.
Region:
A
B
C
D
0.0
0.5
1.0
1.5
FLuc/RenLuc Luminescence

FIGURE 5

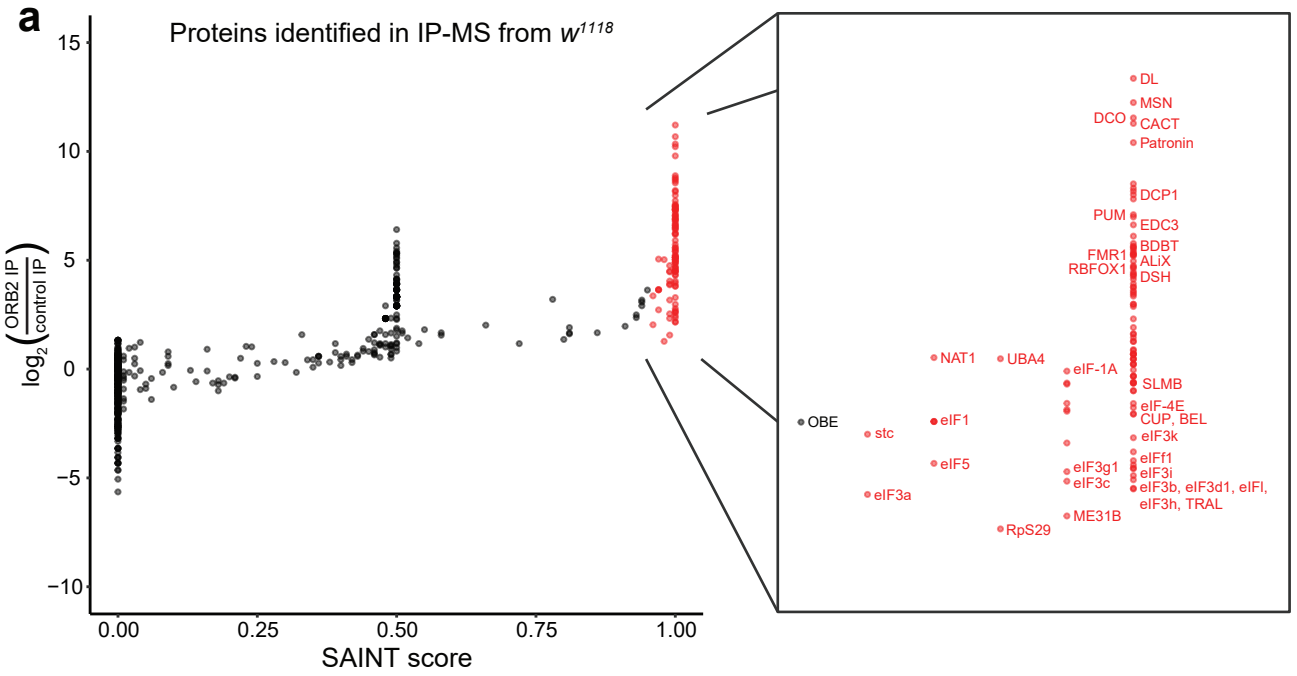
a
Proteins identified in IP-MS from w1118
log2 (ORB2 IP / control IP)
SAINT score
DL
MSN
DCO
CACT
Patronin
DCP1
PUM
EDC3
BDBT
FMR1
ALiX
RBFOX1
DSH
NAT1
UBA4
eIF-1A
SLMB
eIF-4E
CUP, BEL
OBE
stc
eIF1
eIF3k
eIF5
eIFf1
eIF3g1
eIF3i
eIF3c
eIF3b, eIF3d1, eIFI,
eIF3h, TRAL
eIF3a
ME31B
RpS29

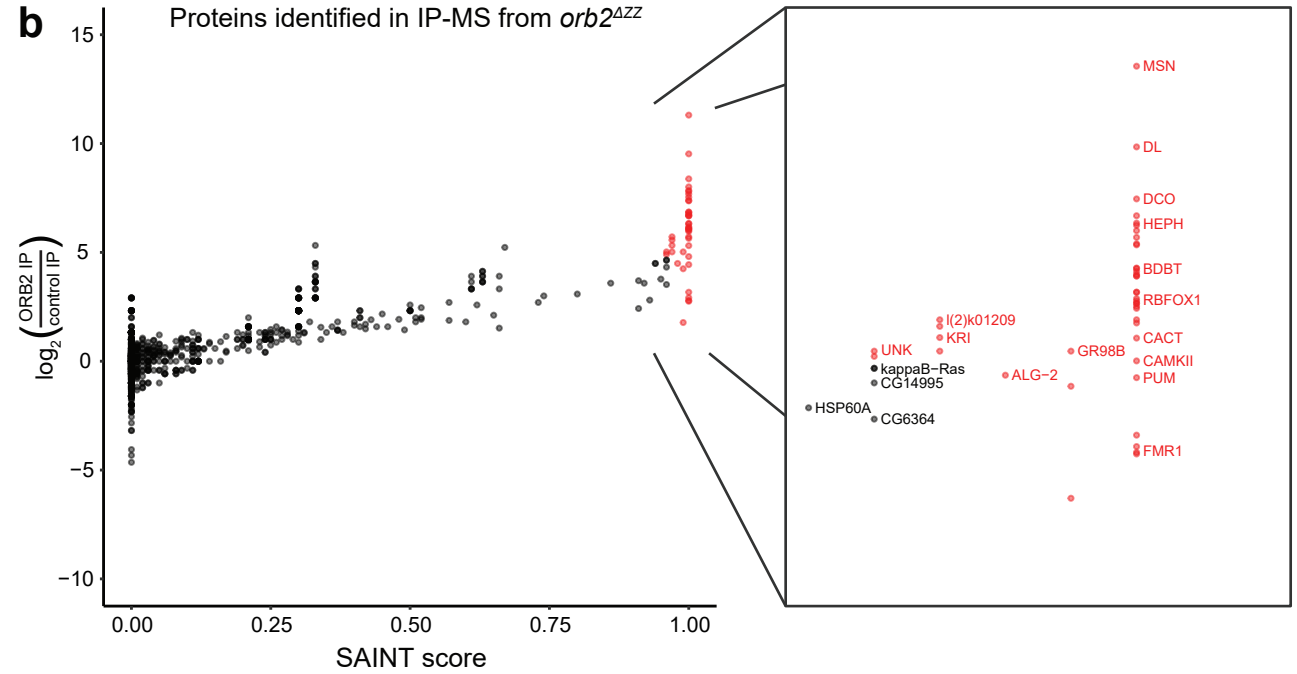
b
Proteins identified in IP-MS from orb2ΔZZ
log2 (ORB2 IP / control IP)
SAINT score
MSN
DL
DCO
HEPH
BDBT
RBFOX1
l(2)k01209
KRI
CACT
UNK
GR98B
CAMKII
kappaB−Ras
ALG−2
PUM
CG14995
HSP60A
CG6364
FMR1

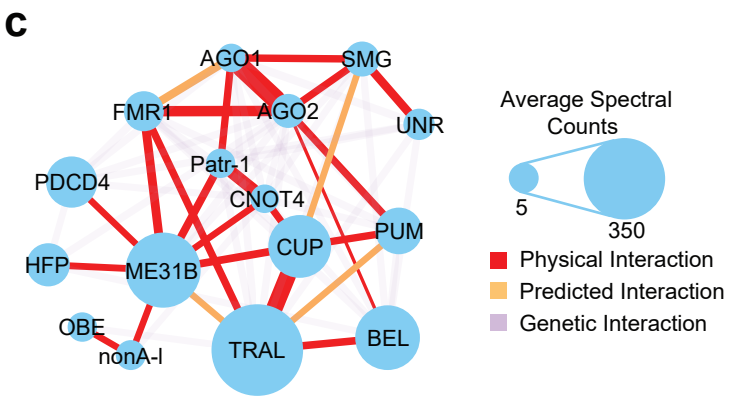
c
AGO1
SMG
FMR1
AGO2
UNR
Patr-1
PDCD4
CNOT4
PUM
CUP
HFP
ME31B
OBE
nonA-I
TRAL
BEL
Average Spectral Counts
5
350
Physical Interaction
Predicted Interaction
Genetic Interaction

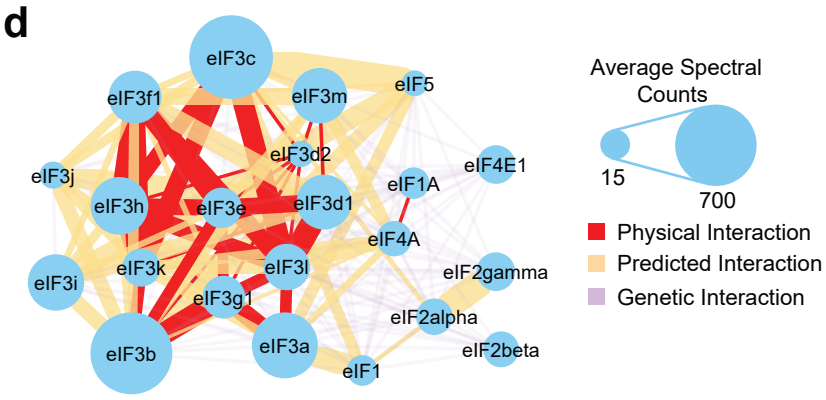
d
eIF3c
eIF3f1
eIF3m
eIF5
eIF3d2
eIF4E1
eIF3j
eIF1A
eIF3h
eIF3e
eIF3d1
eIF4A
eIF3k
eIF3l
eIF2gamma
eIF3i
eIF3g1
eIF2alpha
eIF3b
eIF3a
eIF2beta
eIF1
Average Spectral Counts
15
700
Physical Interaction
Predicted Interaction
Genetic Interaction

FIGURE 6

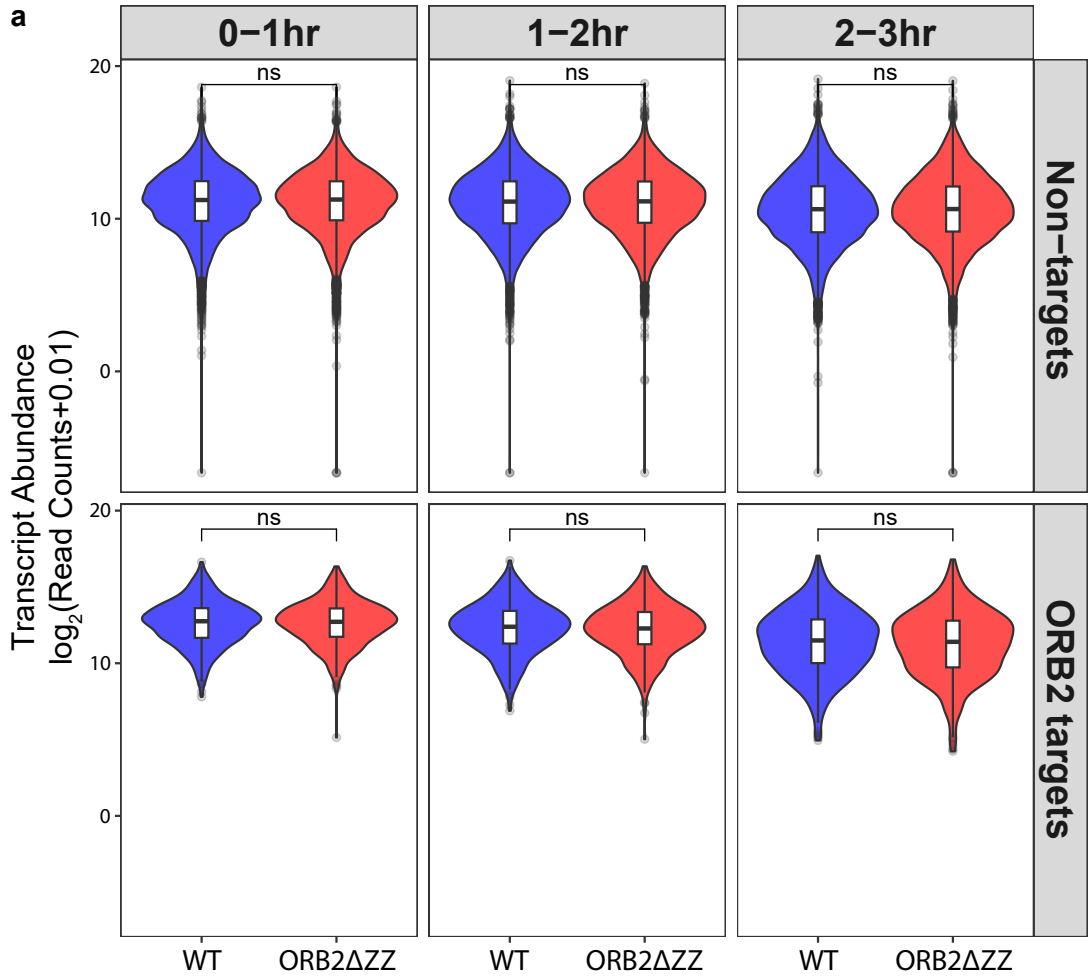
a
0−1hr
1−2hr
2−3hr
Non−targets
ORB2 targets
Transcript Abundance
log2(Read Counts+0.01)
ns
20
10
0
WT
ORB2ΔZZ

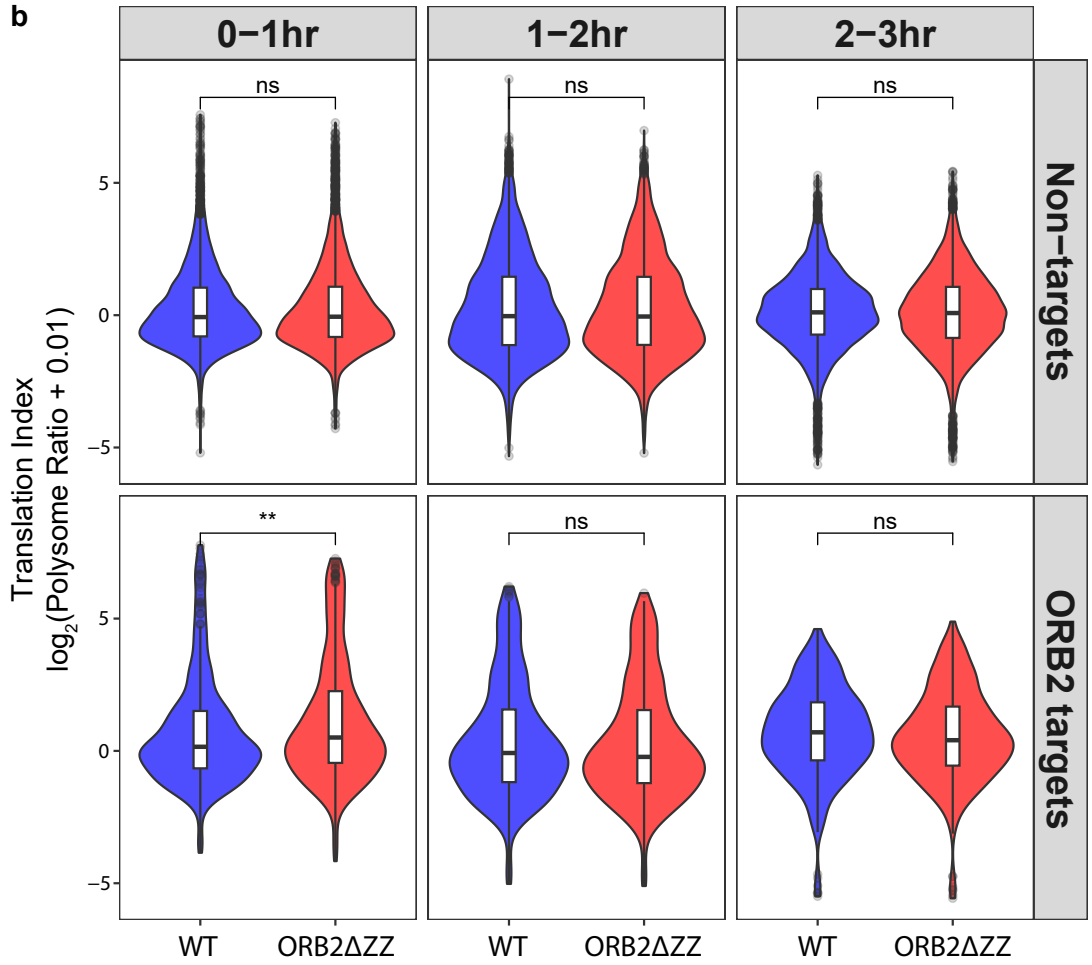
b
0−1hr
1−2hr
2−3hr
Non−targets
ORB2 targets
Translation Index
log2(Polysome Ratio + 0.01)
ns
**
5
0
−5
WT
ORB2ΔZZ

FIGURE 7

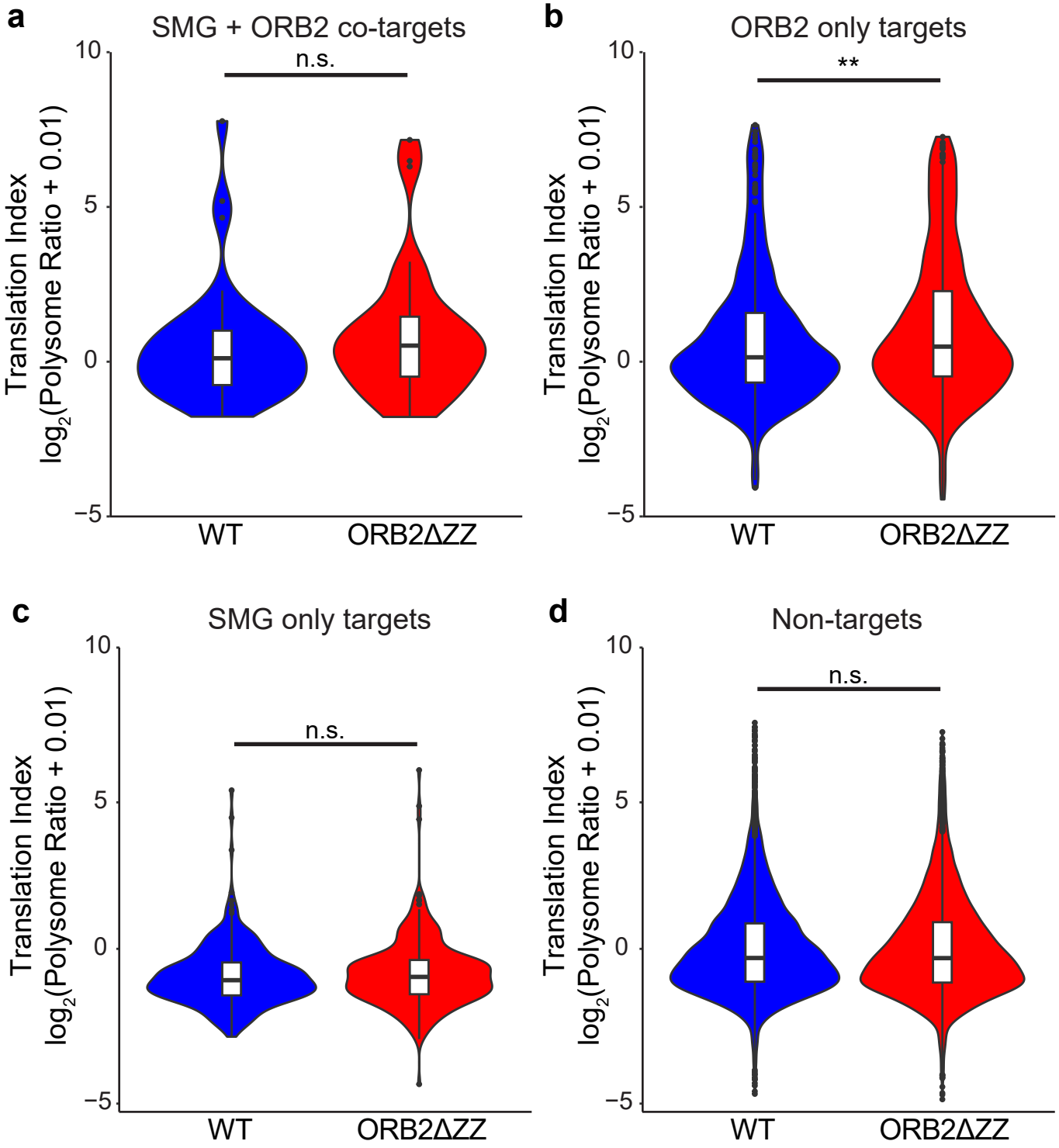
a
SMG + ORB2 co-targets
n.s.
b
ORB2 only targets
**
c
SMG only targets
n.s.
d
Non-targets
n.s.
Translation Index
log2(Polysome Ratio + 0.01)
10
5
0
−5
WT
ORB2ΔZZ

TABLE 1

Comparison	Backgound (Total)	Orb2 Only	Other Only	Overlap	Fisher's Exact p-value	Odds Ratio
Maternal Unstable (Unfertilized eggs, Tadros et al 2007)	3030	172	744	166	2.20E-16	3.849738
Thomsen et al 2010						
Class I (Stable transcripts)	4186	377	1335	35	2.20E-16	0.2334165
Class II (Maternal Decay only)	5108	395	394	36	0.3359	1.181531
Class III (Maternal Decay + Transcription)	5177	392	326	38	0.02109	1.539281
Class IV (Zygotic Decay only)	4332	322	1171	108	0.06763	1.240746
Class V (Both Maternal + Zygotic Decay)	4186	239	1317	191	2.20E-16	2.53962

TABLE 2. Molecular Function

GO Term Name	Adjusted p-value	GO Term Size	ORB2 targets	Overlap
protein binding	1.13E-21	3760	416	229
mRNA 3'-UTR binding	5.78E-11	48	416	17
mRNA binding	1.15E-10	238	416	35
mRNA regulatory element binding translation repressor activity	2.51E-08	18	416	10
translation repressor activity	7.18E-08	25	416	11
translation regulator activity	2.28E-04	106	416	16
catalytic activity, acting on DNA	2.49E-04	147	416	19
protein serine/threonine kinase activity	5.25E-04	184	416	21
DNA binding	6.42E-04	1127	416	69
poly-pyrimidine tract binding	1.28E-03	14	416	6
adenyl ribonucleotide binding	1.42E-03	846	416	55
catalytic activity, acting on a nucleic acid	1.62E-03	406	416	33
ATP binding	2.44E-03	840	416	54
purine ribonucleotide binding	2.99E-03	1021	416	62
purine nucleotide binding	3.63E-03	1072	416	64
adenyl nucleotide binding	3.73E-03	896	416	56
ribonucleotide binding	4.31E-03	1033	416	62

TABLE 3. Biological Process

GO Term Name	adjusted p-value	GO Term Size	ORB2 targets	Overlap
purine ribonucleoside triphosphate binding	4.48E-03	1012	416	61
anatomical structure development	5.77E-28	2775	435	212
developmental process	2.30E-27	2954	435	219
negative regulation of cellular process	1.73E-25	1520	435	144
cell development	6.92E-25	1450	435	139
multicellular organism development	8.26E-25	2276	435	182
cell differentiation	3.46E-24	1768	435	155
cellular component organization	1.07E-21	3178	435	217
regulation of metabolic process	1.81E-21	2253	435	174
gamete generation	1.19E-20	917	435	100
germ cell development	7.67E-20	721	435	86
anatomical structure morphogenesis	1.34E-19	1580	435	136
oogenesis	1.45E-19	582	435	76
system development	5.09E-19	1527	435	132
multicellular organismal reproductive process	1.60E-18	1096	435	107
regulation of primary metabolic process	1.69E-17	1860	435	146
nervous system development	4.18E-17	1196	435	110
animal organ development	5.43E-17	1200	435	110
regulation of macromolecule biosynthetic process	1.09E-15	1742	435	136

TABLE 4. Cellular Component

GO Term Name	adjusted p-value	GO Term Size	ORB2 targets	Overlap
nucleus	1.99E-14	3234	438	196
ribonucleoprotein granule	2.57E-12	119	438	27
cytoplasmic ribonucleoprotein granule	7.11E-12	114	438	26
cellular anatomical structure	6.48E-10	10708	438	426
cytoplasm	6.02E-09	5187	438	255
P granule	1.14E-07	46	438	14
cytosol	1.14E-07	1131	438	82
germ plasm	2.15E-07	48	438	14
nucleoplasm	1.40E-06	573	438	50
pole plasm	2.54E-06	57	438	14
nuclear lumen	3.31E-06	910	438	67
cytoplasmic stress granule	5.07E-06	21	438	9
protein-containing complex	2.53E-05	2861	438	151
chromosome	3.50E-05	787	438	58
PcG protein complex	8.68E-04	27	438	8
transferase complex	2.13E-03	550	438	41
intracellular protein-containing complex	4.15E-03	625	438	44
cell junction	4.67E-03	608	438	43
intracellular organelle lumen	4.94E-03	1158	438	69
membrane-enclosed lumen	5.08E-03	1159	438	69
organelle lumen	5.08E-03	1159	438	69
cell cortex	5.36E-03	208	438	21

TABLE 5

Comparison	Backgound	Orb2 Only	Other Only	Overlap	Fisher's Exact p-value	Odds Ratio
Smaug (Chen et al 2012)	3758	254	290	41	0.0001416	2.09148
Brat (Laver et al 2015)	3347	228	701	69	0.02181	1.40294
Pum (Laver et al 2015)	3696	238	352	57	6.197E-08	2.51398
Rin (Laver et al 2020)	4429	365	507	6	2.15E-10	0.14363